SUPPLEMENTARY MATERIAL

The molecular structural diversity of mitochondrial cardiolipins

Gregor Oemer[a], Katharina Lackner[a], Katharina Muigg[a], Gerhard Krumschnabel[b], Katrin Watschinger[c], Sabrina Sailer[c], Herbert Lindner[d], Erich Gnaiger[b], Saskia B. Wortmann[e], Ernst R. Werner[c], Johannes Zschocke[a], and Markus A. Keller[a,1]

[a]Division of Human Genetics, Medical University of Innsbruck, 6020 Innsbruck, Austria; [b]Oroboros Instruments Corporation, 6020 Innsbruck, Austria; [c]Division of Biological Chemistry, Biocenter, Medical University of Innsbruck, 6020 Innsbruck, Austria; [d]Division of Clinical Biochemistry, Biocenter, Medical University of Innsbruck, 6020 Innsbruck, Austria; and [e]Department of Paediatrics, Salzburger Landeskliniken, Paracelsus Medical University, 5020 Salzburg, Austria

[1]To whom correspondence should be addressed. Email: markus.keller@i-med.ac.at.

Supplemental Dataset 2: Script for mathematical modelling of tandem mass spectrometric data with R ("Script_1_MS2_Fragment_Modeling_Analysis.txt").

Supplemental Dataset 3: Script for modeling of fatty acyl profiles and their visualization in R ("Script_2_Fatty_Acyl_Modeling.txt").

Supplemental Text S1: Cardiolipin species nomenclature in this study

Cardiolipins (CL) can be defined on different structural levels. While CL72 is a collective term for all CL molecules with 72 side chain carbon atoms, CL72:4 defines more precisely the presence of 4 double bonds. With CL18:1_18:1_18:1_18:1, additional information is given on length and saturation on all four individual fatty acyls (FA). Still, this molecule can correspond to achiral (FA and double bonds distributed symmetrically) or chiral molecular CL species. Thus further specifications include exact double bond positions and the substitution order of FA along the CL backbone. Each CL consists of two phosphatidic acid (PA) subunits with two FA side chains, which can be structurally described similarly to CL (e.g. PA36, PA36:2, or PA18:1_18:1). For the systematic CL naming system see http://www.lipidmaps.org (1).

Supplemental Text S2: HPLC-MS/MS method development and validation

The LC-MS/MS method presented here was optimized to allow a clear chromatographic separation of up to 135 different CL mass-species within 12 minutes and their MS1 based quantitation as single charged ions in the mass range of 1100-1600 m/z (Fig. 1A, see Methods). Single charged species have the advantage that their higher mass separates them well from other phospholipids. With the here used parameters, we observed no detectable double charged species. Highly ordered elution profiles are thus generated, allowing straight-forward identification and annotation of CL species orienting along commercially available standards. Approximately 10% of the total CL mass occurred as sodium adducts. Peaks were quantified by summing the counts of each monoisotopic and first isotopic mass. This allowed relative quantification of individual CLs as characterized by their total carbon chain length and double bond count (Fig. 1B). The elution profiles of individual peaks indicated the presence of several isobaric CL subspecies with only slightly differing chromatographic behavior (Fig. 1C). These differences are caused by variable FA substitutions, generating different molecular CL species with the same total carbon chain length and number of double bonds.

Absolute quantification was achieved by linear regression analysis with externally measured dilution series of commercially available standards ($CL(14:0)_4$, $CL(18:1)_4$) and normalization via the internal standard (ISTD) $CL(14:0)_4$. Cardiolipins were perfectly soluble in LC-MS/MS starting condition (38% mobile phase A, 62% mobile phase B: 55.8% isopropanol / 29% acetonitrile, 15.2%H_2O). We observed a LOD of 77.1 fmol and a LOQ of 177.7 fmol and a linear behavior in the concentration range between the LOQ and 10 nmol (Fig. S1A, R^2= 0.99) (126 CL m/z traces in 12 blank samples were used for calculation). A washing step (99% LM B, 4 min, 0.6 ml/min flow rate) at the end of each run prevented carryover in the regular measured blank samples (see LOD/LOQ calculation). Ionization efficiencies between $CL(14:0)_4$ and $CL(18:1)_4$ were highly similar (Fig. S1A), indicating that the same calibration curves can be applied to a variety of CL species. In order to test the precision of our method and to evaluate storage properties of lipid extracts we repeatedly measured aliquots of the same samples in week 1, 2, 3, and 5 and quantified all respective CL profiles (Fig. S1B). We found that the intra-assay CVs were well below 10% in the first 3 weeks after extraction and in the range of 5.3-7.5% when only accounting for CL species that constitute 95% of the total CL mass (Fig. S2A). CV values for minor CL species that are closer to the LOQ are typically higher than for major CLs as illustrated by a cumulative CV value calculation from high to low abundant species (Fig. S2B). The inter-assay CV was 16.8% for absolute quantities and 7.1% for CL profiles within the first 3 weeks and increased to 21.1% when including week 5 measurements (Fig. S2C). These results suggest that measurements of samples should be performed quickly after extraction. For all further experiments we typically subjected samples to LC-MS/MS analysis within 1-3 days after extraction (storage at -20°C in lyophilized state). Furthermore, in spiking experiments with 50 and 200 pmol $CL(18:1)_4$ we obtained recovery rates of 100.0 ± 3.0% and 100.6 ± 9.0% respectively (Fig. S2D).

Supplementary Text S3: **The conditional reconfiguration of cardiolipin compositions.**

From the obtained organism data set (Fig. 5 and S15) we chose three examples to illustrate the spectrum of biologically relevant cardiolipin compositions that is generated upon the concert action of the environment, growth parameters, and the differential regulation of phospholipid metabolism in tissues:

Example 1: When comparing the cardiolipin compositions in tissues (brain, heart and liver) obtained from mouse and pig, we quantified high profile similarities between the individual organs, whereas species specific differences were only secondary (Fig. S16A-B). This indicates that the cardiolipin composition in mammalian tissues is likely controlled by an evolutionary conserved and organ-specific regulatory principle that is underlying cardiolipin and phospholipid metabolism. Furthermore, our fatty acyl modeling results suggested that the buildings blocks of cardiolipins in heart and liver are dominated by linoleic acid, while brain cardiolipins are often composed of oleic acid in combination with arachidonic acid (FA20:4) and docosahexaenoic acid (FA22:6) (Fig. S16C).

Example 2: Cardiolipin compositions reconfigure in a growth condition dependent manner in *Escherichia coli*. It has been established that the bacterial cardiolipin content is modulated under different growth conditions, growth phases, and in response to stressors (4, 5). When comparing the cardiolipin compositions measured in E.coli grown in minimal M9 medium versus nutritionally rich LB medium, we observe clearly altered cardiolipin patterns as well as an increased total cardiolipin content in M9 medium, where glucose represents the sole carbon source (Fig. S17A-B). Growth conditions were well separated in a principal component analysis on basis of all individual cardiolipin species (Fig. S17C), with a broad carbon chain length distribution in LB medium and CL66 and CL68 levels dominating in M9 derived samples (Fig. S17C). Interestingly, bacterial CL66:2 is largely constituted of two PA33:1 phosphatidylglycerol subunits in the M9 condition, whereas the respective isobaric cardiolipin species in eukaryotes mainly contains dimers of PA32:1 and PA34:1. As a consequence also respective fatty acyl profiles exhibit increased levels of fatty acids with uneven carbon numbers (15/17), which are likely corresponding to cyclopropane-containing fatty acids. The present fatty acyl modeling approach, however, is not able to distinguish isobaric trans-, cis-, and cyclopropane-fatty acids, such as for example FA17:0(cyclo 9-10) and FA18:1, which are therefore subsumed within the same mass-species.

Example 3: The conditional remodeling of cardiolipin composition can also be observed during batch culture growth of *Saccharomyces cerevisiae*. While in logarithmic growth phase (OD=1.5, 7h) the

major cardiolipin species CL64/66/68/70 exhibit a broad double bond distribution ranging from 2 to 4 double bonds, a clear shift towards cardiolipin species with 4 double bonds was measured after 48h of batch culture growth (OD=5.9, Fig. S18A-B), an enrichment that is also apparent when cardiolipin profiles are projected onto their respective double bond component (Fig. S18C-D). Analysis on the fatty acyl profile level suggests that this effect is largely driven by the gradual depletion of FA16:0, while FA16:1 and FA18:1 represent the major fatty acyls at an equimolar ratio (Fig. S18E). The cardiolipin diversity after 48h can thus to a large part be explained by stochastic combination of these two major fatty acids (Fig. S18F).

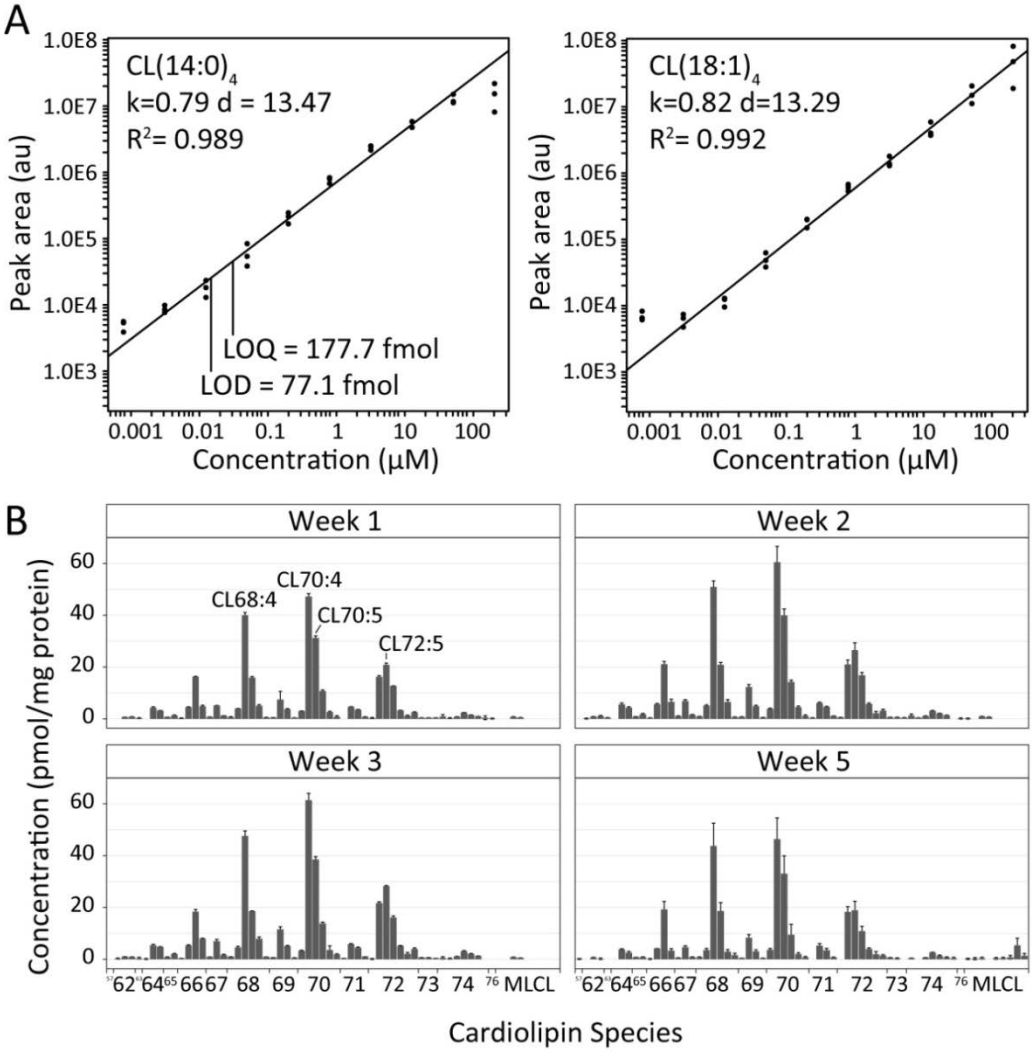

Supplemental Figure 1: ***Linear range, limit of detection/ quantification and intermediate precition****. (A) Standard dilution series of CL(14:0)$_4$ and CL(18:1)$_4$ were linear below 100 µM (1 nmol) and allowed determining a limit of detection (LOD) of 77.1 fmol and a limit of quantification (LOQ) of 177.7 fmol. (B) Repeated measurement of aliquots of the same samples revealed highly similar profiles after 1, 2, 3 and 5 weeks (see Fig. S1 for CV analysis).*

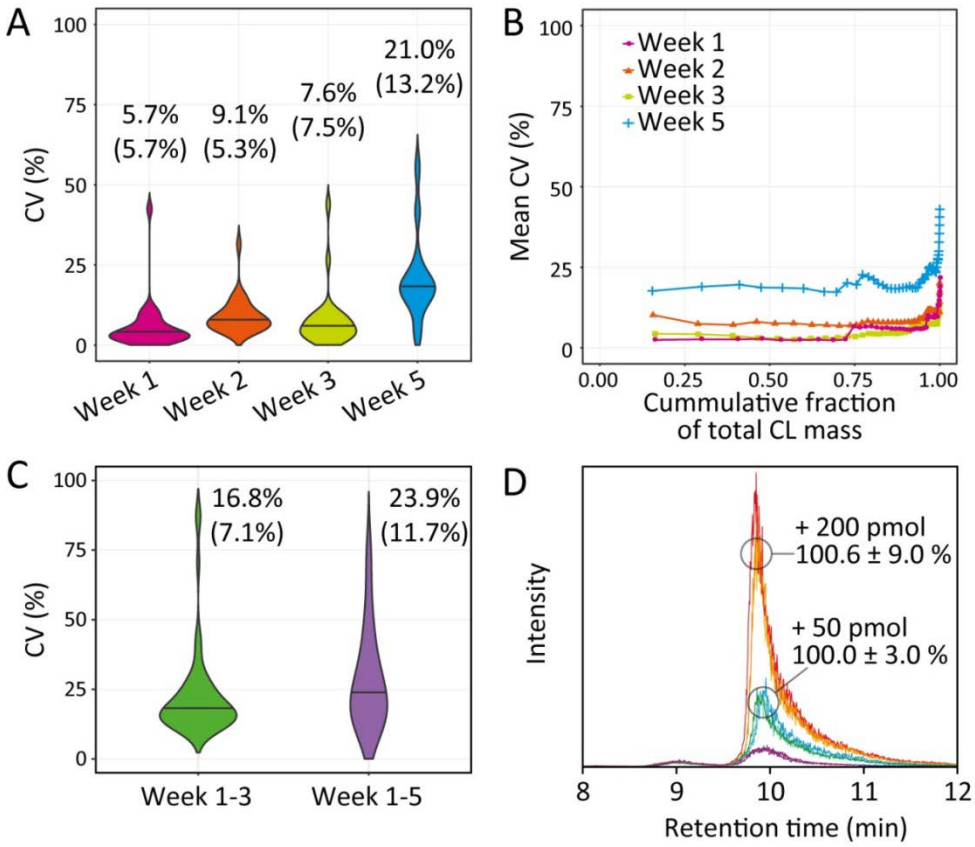

Supplemental Figure 2: ***Repeatability, intermediate precision, accuracy and recovery of cardiolipin quantification****. (**A**) Violin plots of the intra-assay coefficients of variation (CV) were calculated for all cardiolipin species that constitute 95% of the total cardiolipin mass. One plot is given for each measurement week. Mean CVs for quantitative data are indicated above each plot. Mean CVs for data after conversion into normalized profiles are plotted in brackets. (**B**) Cumulative CV calculation by integrating cardiolipin species according to their abundance. The increment of the Mean CV when also incorporating low abundant cardiolipin species results from their higher CVs. (**C**) Interassay CVs were calculated for week 1-3 and week 1-5 independently and are illustrated as described in (B). (**D**) Recovery of RAW 264.7 lipid extracts (violett chromatograms) spiked with 50 (blue) and 200 pmol (orange) mixtures of CL14:0/14:0/14:0/14:0 and CL18:1/18:1/18:1/18:1. Recovery values are given as mean ± sd (n=3).*

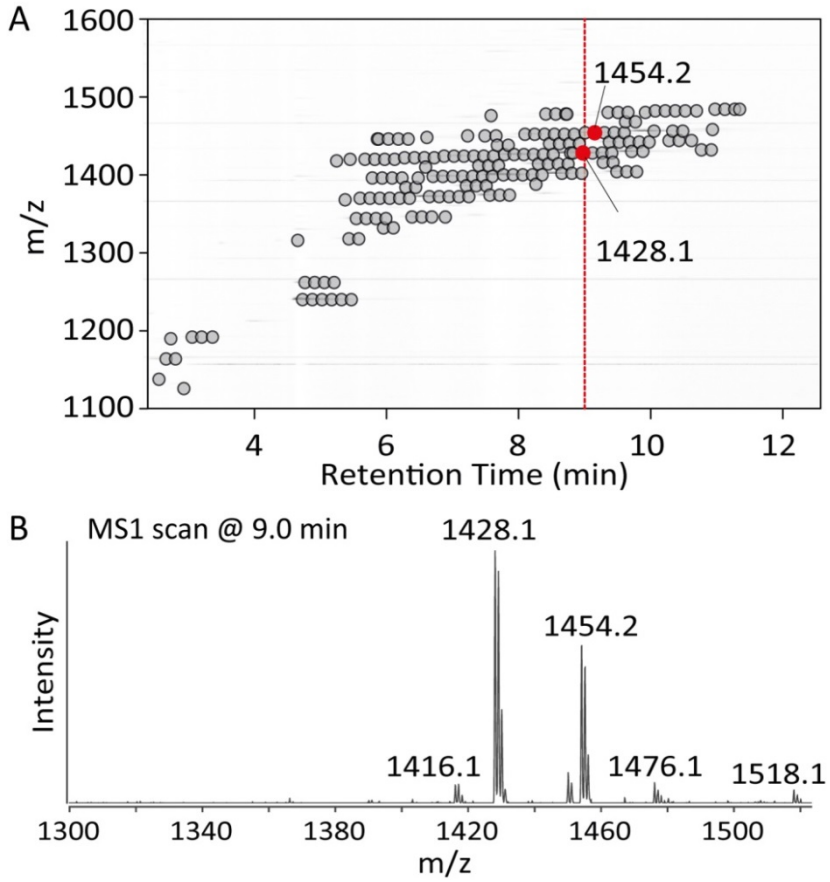

Supplemental Figure 3: ***Cardiolipin fragmentation experiments****. (**A**) Cardiolipin chromatographic elution profile depicting the fragmental spectra recorded in the course of this measurement (Grey and red dots). Red dashed line indicates the MS2 scans recorded around RT=9 min. (**B**) Mass spectrum of a RAW 264.7 lipid extract at retention time of 9.0 min. Several lipid species co-elute, with the CLs corresponding to 1428.1 and 1454.2 m/z being the two most abundant. Based on this spectrum relevant CLs are automatically identified and selected for data dependent acquisition of MS2 spectra.*

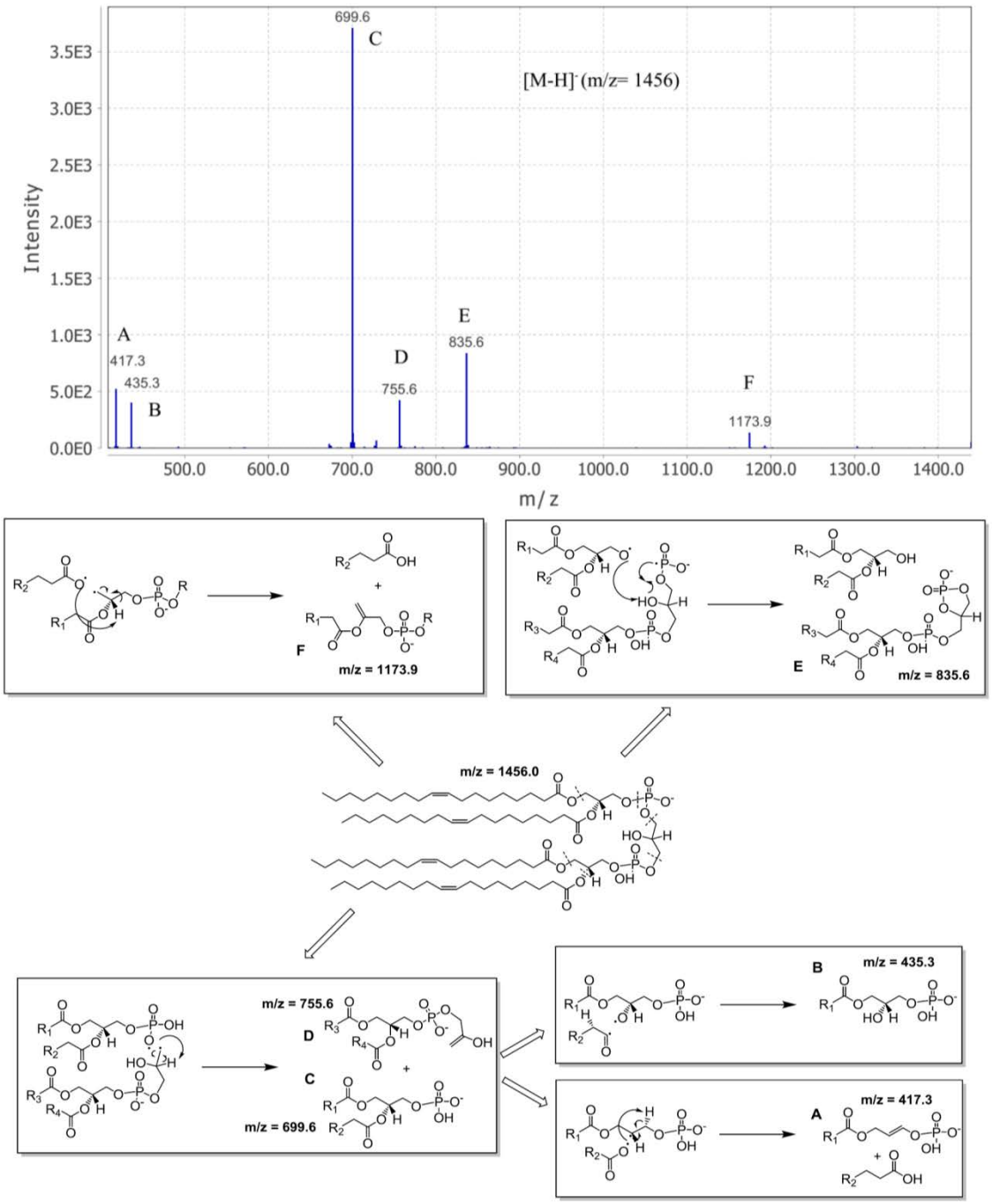

Supplemental Figure 4: ***Cardiolipin fragmentation paths****. Top panel: Exemplary MS/MS fragment spectrum of CL(18:1)$_4$ ([M-H]$^-$ = 1456.0 m/z) at a collision energy for CID of 38%. Major fragments A-F are formed. Bottom panel: Potential fragmentation mechanisms of the 6 most intense fragments. The top left shows cleavage of a fatty acyl and generation of fragment F. Fragment E is formed by backbone fragmentation and release of a diacylglycerol (top right). The bottom left shows backbone fragmentation at the bridging glycerol and generation of fragments D and C, which can further fragment into A and B by cleavage of a fatty acyl residue.*

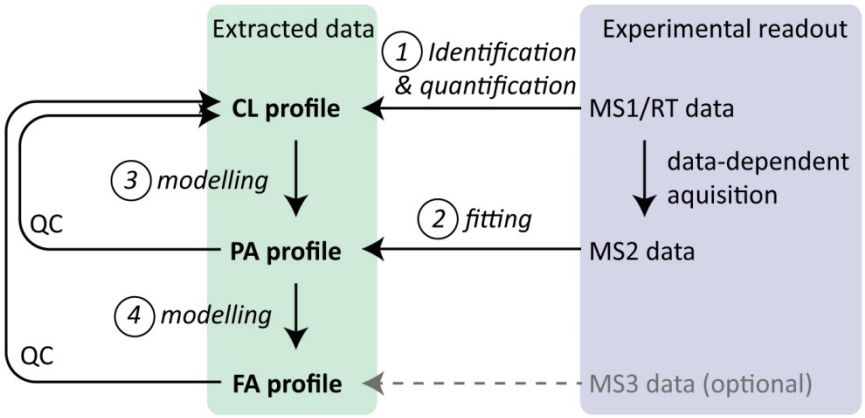

Supplemental Figure 5: ***General data analysis strategy****: MS1 data is used for cardiolipin identification and quantification (Fig. 1B), MS2 for extracting and solving PA profiles (Fig. 2B). PA->FA modeling allows predicting individual FA compositions. FA->CL and PA->CL prediction using stochastic and symmetric CL construction models serveed as internal quality control (QC) for the extracted data.*

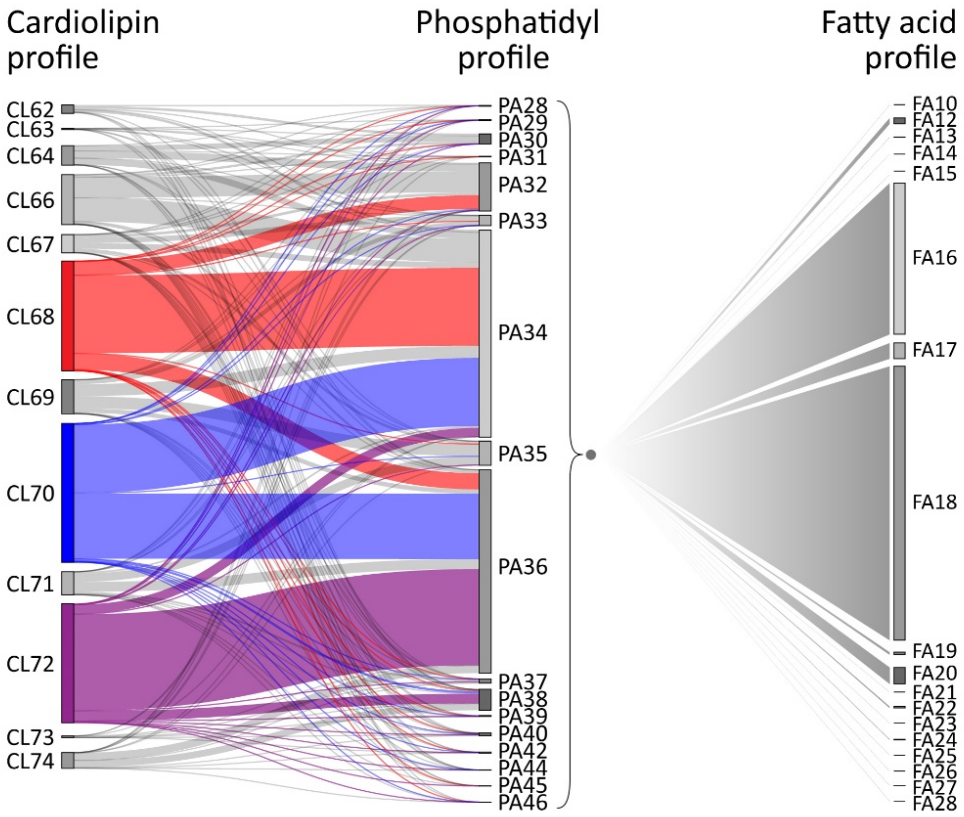

Supplemental Figure 6: ***Structural characterization of the cardiolipin composition in a RAW cell pellet projected on the carbon chain length component.*** *MS2 fragment data was used for computational modeling of underlying phosphatidic acid (PA) profiles. The structural composition of each cardiolipin molecule thus results from combination of two PA subunits. The total pool of CL72 (violet) is thus composed to 80% of PA36/PA36, but also from PA34/PA38 and other combinations. The same refers to CL70 (blue) and CL68 (red). The cumulative PA profile was then used to determine the fatty acid (FA) composition incorporated into cardiolipins by mathematical modeling (see Methods).*

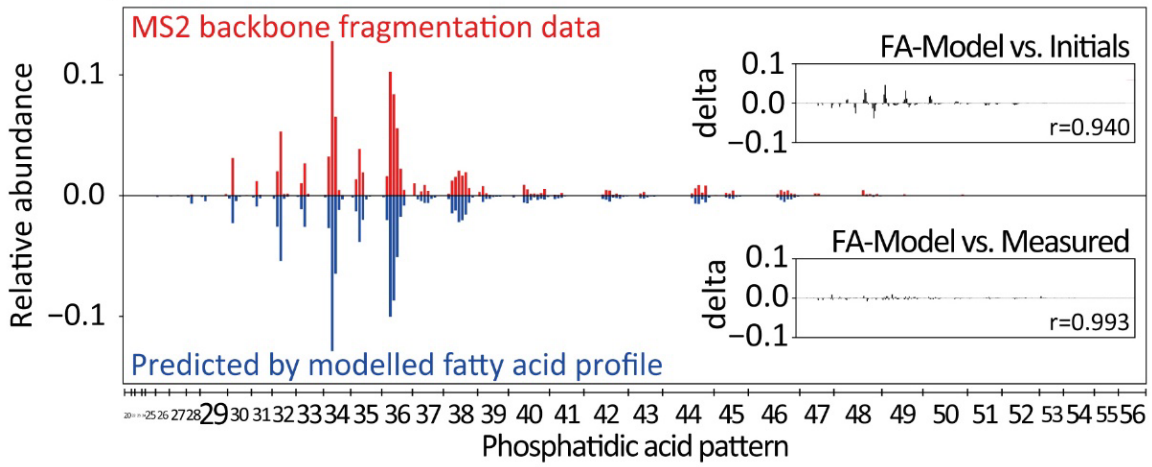

Supplemental Figure 7: ***Fatty acyl profile validation.*** *PA profiles are computationally generated from FA composition results (blue bars) and are related to the PA profiles extracted from MS2 data (red bars) to evaluate the quality of FA modeling. The FA profile results explain PA patterns with high accuracy and were superior to an initial FA profile estimation that bases on projecting PA species on their main theoretical FAs (Pearson correlation coefficients of 0.993 and 0.940, respectively).*

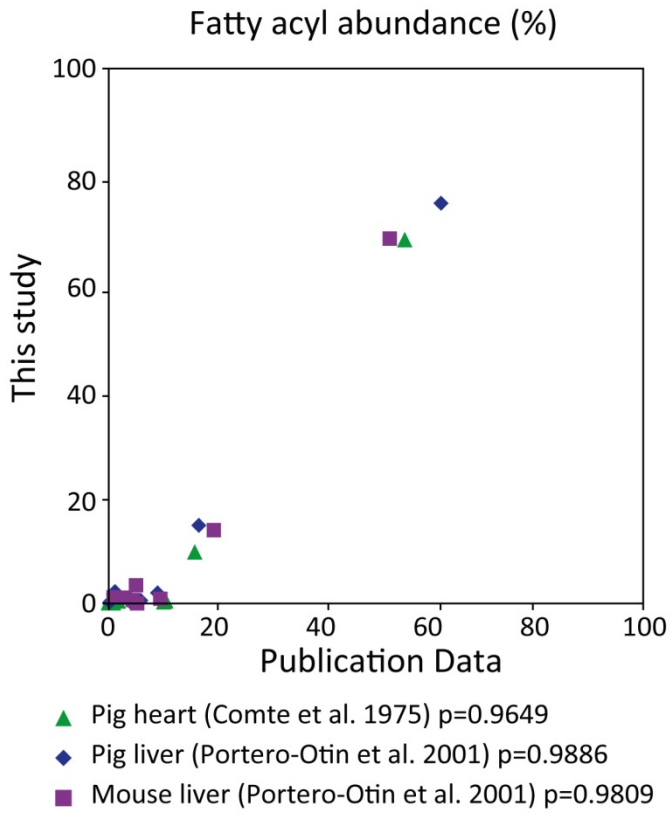

Supplemental Figure 8: ***Confirmation of fatty acid profile validity.*** *Fatty acyl profiles quantified in pig and mouse tissues were compared to available literature data. Data of this study is plotted against values extracted from* (2, 3). *Pearson correlation analysis revealed good agreement between each of the pairs of fatty acyl profiles (p > 0.95).*

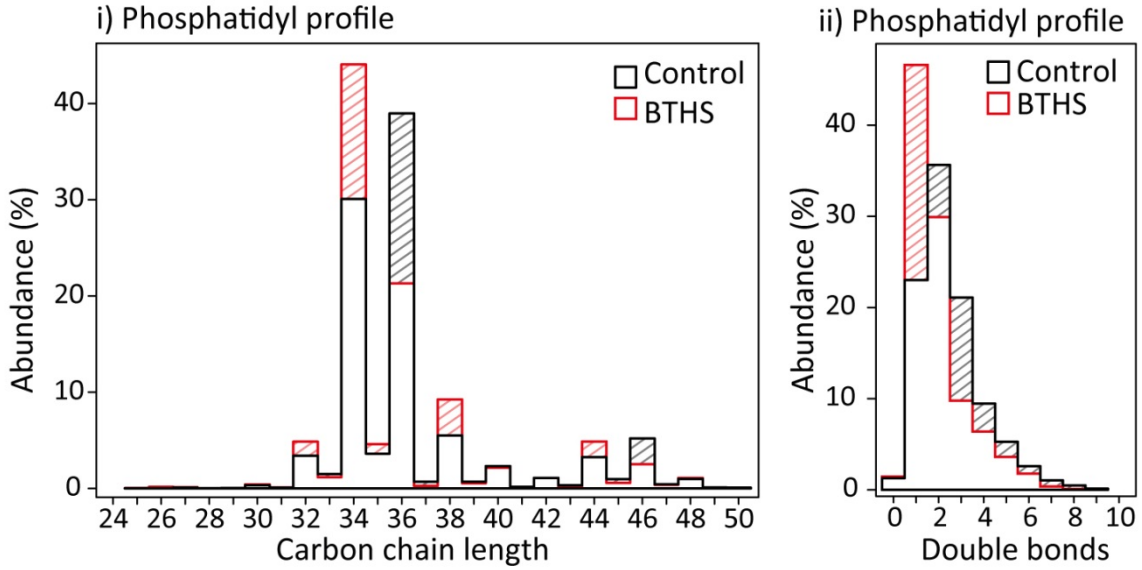

Supplemental Figure 9: ***Phosphatidyl profiles in BTHS patients and controls.*** ***(i)*** *The side chain length distribution exhibits lower carbon numbers in BTHS phosphatidic acid units and* ***(ii)*** *the double bond distribution is shifted towards a higher degree of saturation when compared to unaffected control fibroblasts.*

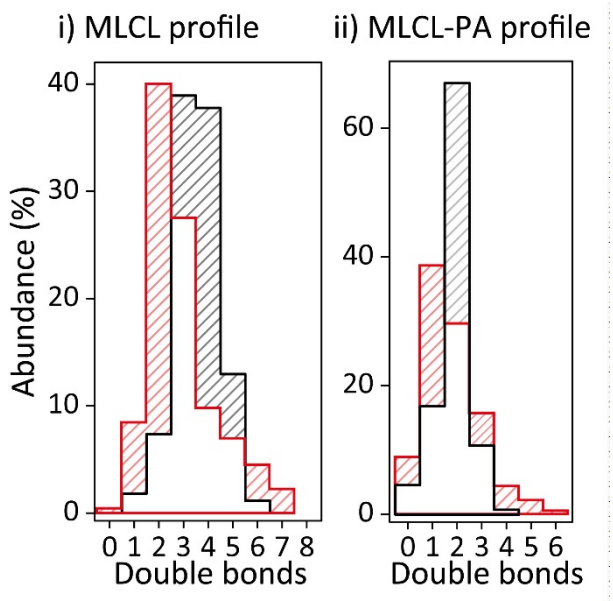

Supplemental Figure 10: ***Monolyso-cardiolipin (MLCL) composition in BTHS patient cells and controls****. In analogy to cardiolipins (Fig. 3) also for MLCLs* ***(i)*** *the side chain length distribution is shifted to lower carbon numbers and* ***(ii)*** *the number of double bonds is decreased when comparing BTHS patient cells with control fibroblasts.*

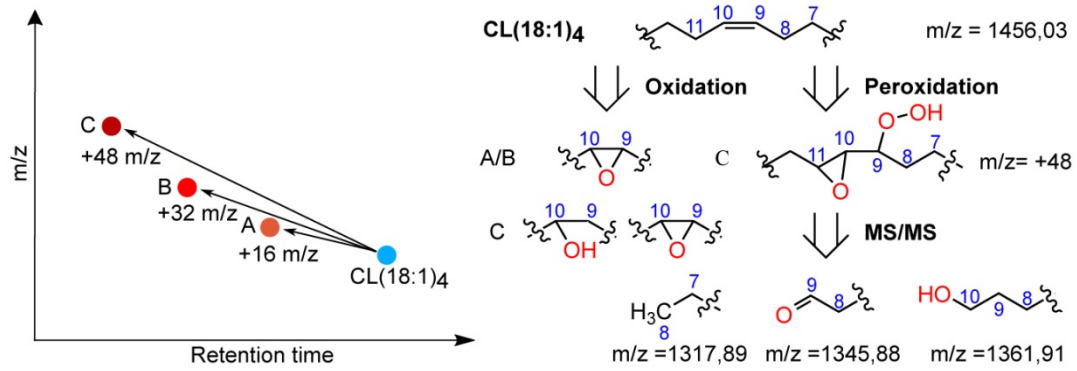

Supplemental Figure 11: ***Cardiolipins with (per)oxidized fatty acyl side chains can be readily detected by HPLC-MS.*** *Chemical oxidation of the commercially available cardiolipin standard CL(18:1)$_4$ with H_2O_2 revealed the following behavior of oxidations products in our HPLC-MS/MS assay: Oxidation or peroxidation of cardiolipin side chains results in both, a shift to earlier retention times due to the more polar character of the product and to an increased m/z. Formation of an epoxide increases the measured mass by 16 (A) or 32 in the case of two oxidation events (B). Mixed integration of hydroxyl and epoxy groups results in +50 m/z. Peroxidation events typically generated mass shifts of +48 (C) and +96 m/z and impacted on the fragmentation behavior of affected cardiolipin molecules by favoring CID cleavage at the affected side chain positions.*

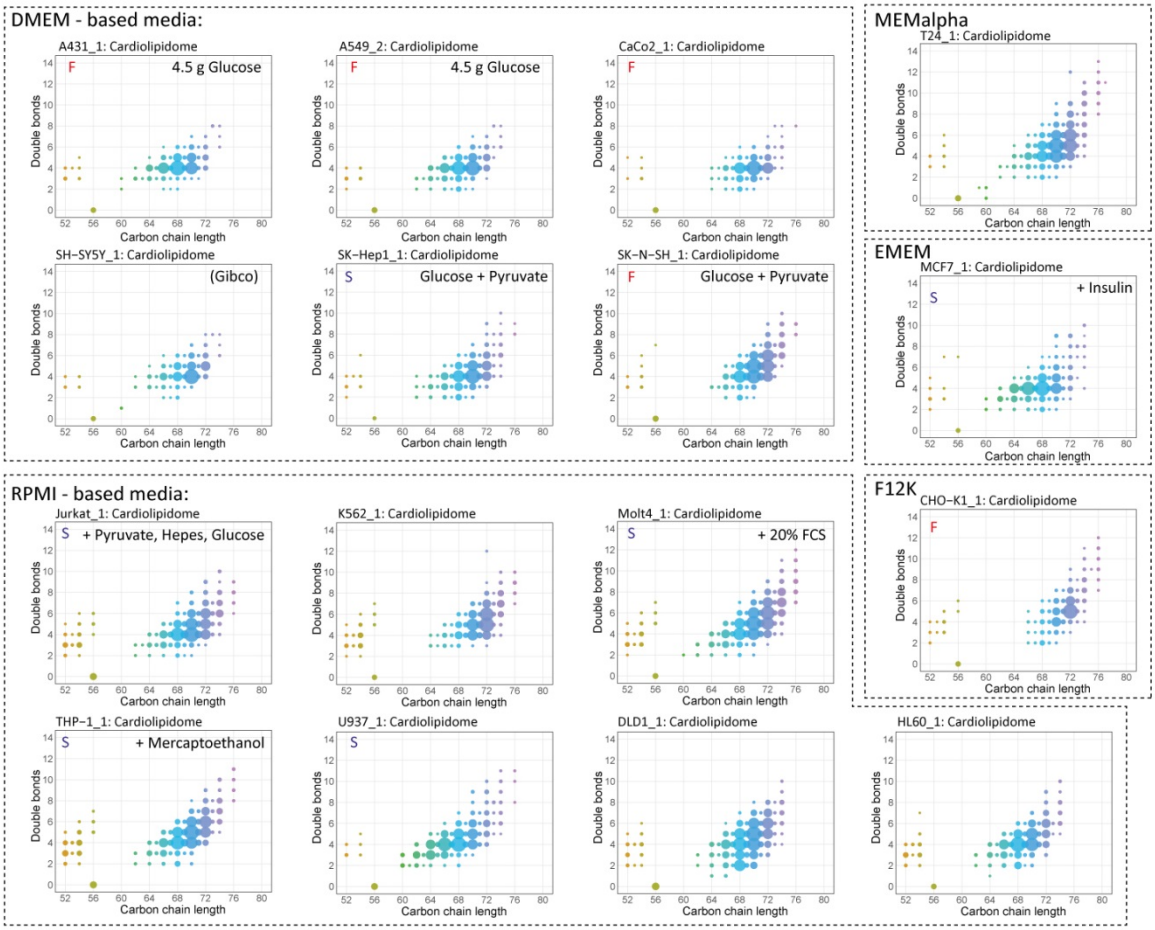

Supplemental Figure 12: ***Integrated peak area data plots for 16 human cell line analyzed for their cardiolipin profiles****. Each panel represents the results obtained for one representative sample per cell line. Integrated peak areas of the first two cardiolipin isotope traces are added and projected back onto their respective carbon chain length and double bond components. Circle sizes indicate the cardiolipin species peak areas, fill color corresponds to the respective total number of side chain carbons. The internal standard (ISTD) is shown in green. Cell culture media formulation and additives (whenever applicable) are indicated.*

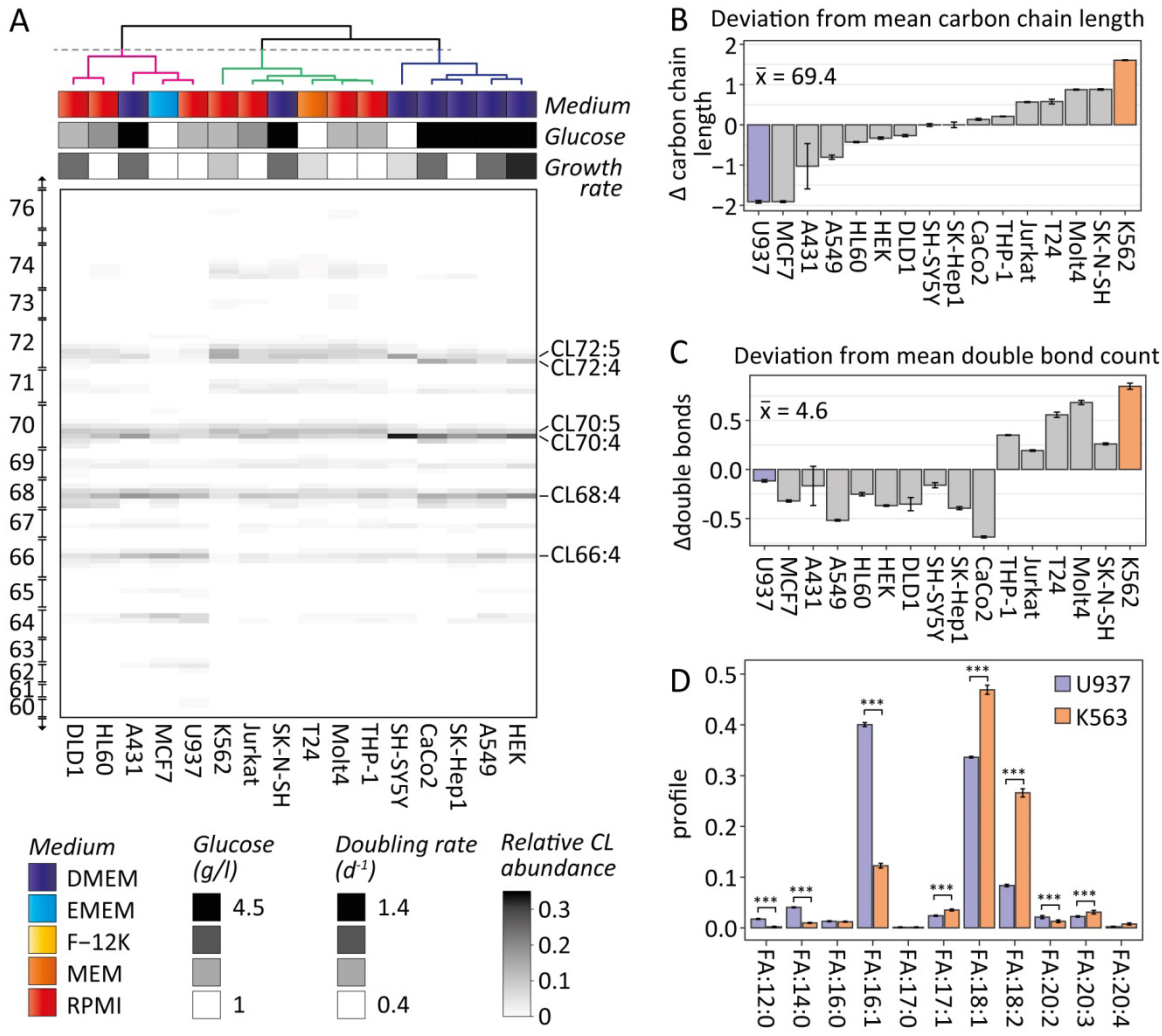

Supplemental Figure 13: ***Cardiolipin heterogeneity in cultured human cell lines.*** *(**A**) 16 human cell lines were grown under their recommended conditions (n=3-4, see Table S1) and CL compositions were quantified. As illustrated as heatmap, mean CL profiles do differ between cell lines. Pearson correlation followed by hierarchical clustering divides cell lines into three clusters (Dendrogram: pink, green, blue). Annotation shows medium, glucose, and estimated growth rate information. (**B**) Mean carbon side chain lengths were calculated for each tested cell line spanning from 67.5 to 71.3 and are depicted as deviation from the overall mean (69.4). (**C**) Same as (B) but for the mean double bond count. (**D**) U937 and K563 were selected as extreme cases and their FA compositions were compared. Two-way Anova was conducted on the influence of two variables (Cell line, FA). The main effect for FA profiles an F ratio of F(112,1) = 15530.9257, p<2e-16. Post hoc Bonferroni corrected analysis revealed 11/112 possible FAs being significantly (< 0.05) altered. Main differences were thus identified as an increased abundance of FA16:1 (p<1e-99) and FA14:0 (p<1e-99) in U937 cells, and a simultaneous decrease of FA17:1 (p=1.67e-15), FA18:1 (p<1e-99) and FA18:2 (p<1e-99) levels.*

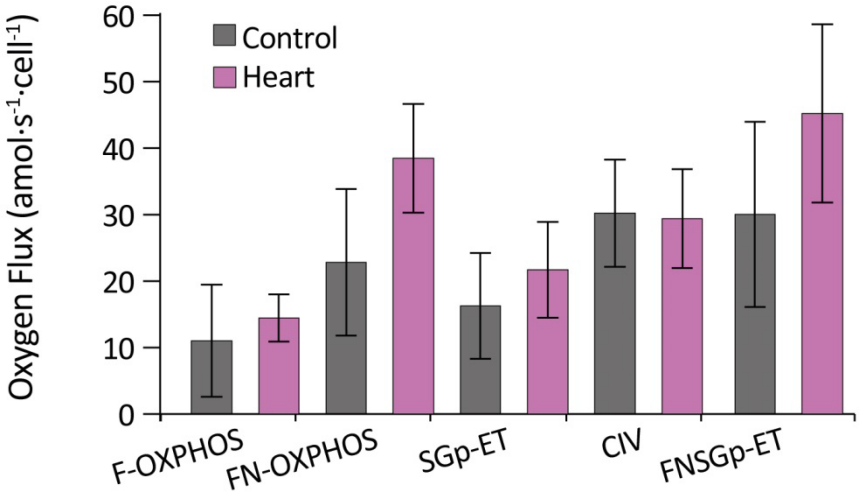

Supplemental Figure 14: ***Respirometic analysis of supplemented HeLa cells.*** *Oxygen flow in permeabilized HeLa cells grown in lipid and serum free (Control) and pig heart lipids supplemented (Heart) conditions. Consecutive substrate-uncoupler-inhibitor titrations allowed analyzing different mitochondrial functional parameters (See extended protocol), including beta-oxidation of fatty acids (F-OXPHOS), combined F- and NADH-linked OXPHOS-capacity (FN-OXPHOS), succinate- and glycerophosphate-supported ET-capacity after inhibition with rotenone and uncoupler titration (SGp-ET), Complex IV activity (CIV) and electron transfer-pathway capacity in the combined FNSGp-pathway (FNSGp-ET). While all observed changes were non-significant (n=4, Bonferroni-adjusted with m=14), we observed a consistent increase of NADH-linked respiratory capacity, which was investigated in detail in subsequent experiments (Fig.4E).*

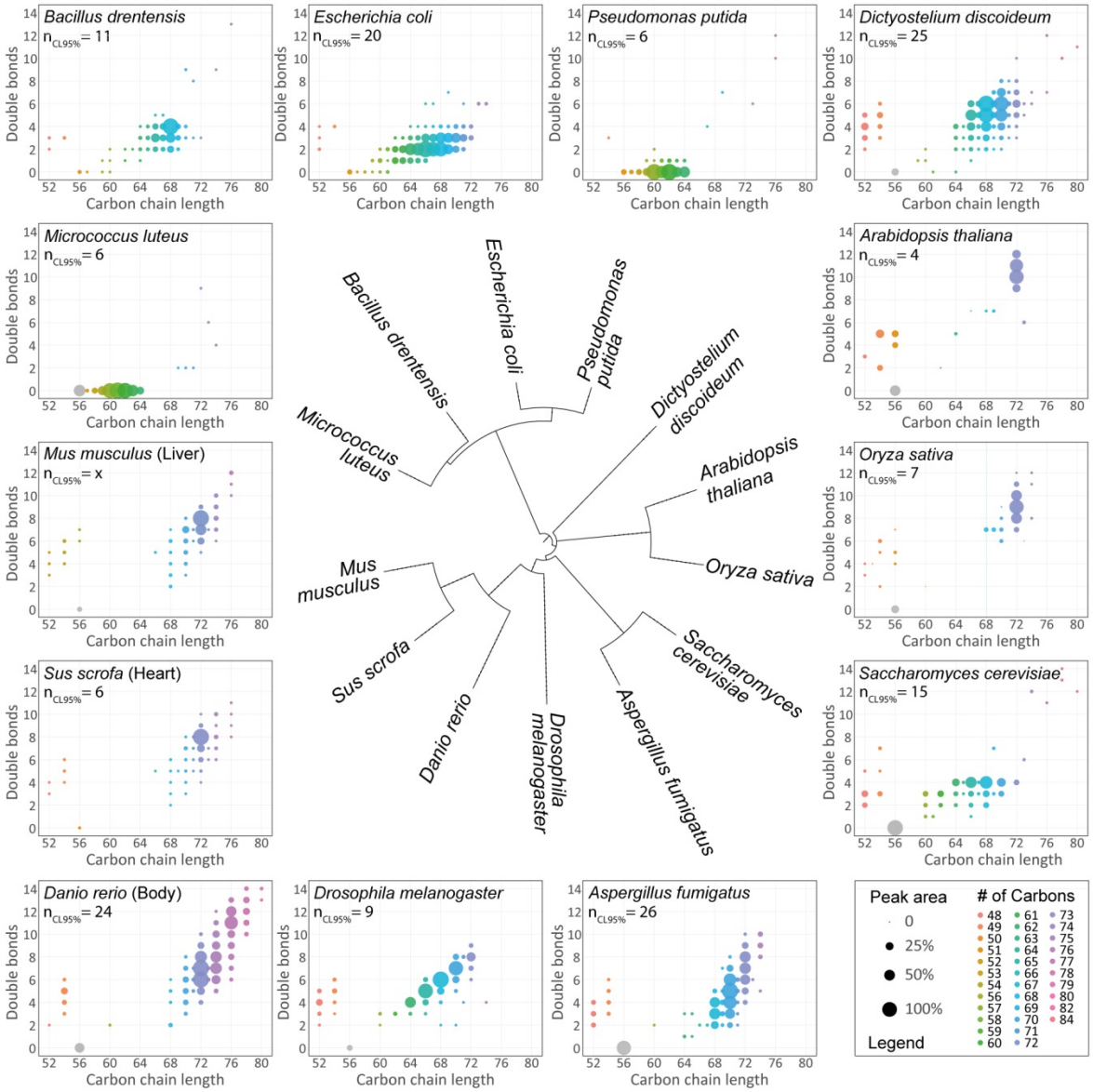

Supplemental Figure 15: ***Characterizing the CL composition of organisms across the domains of life****. CLs were characterized in 13 different organisms. For some species different tissues, growth conditions, sex, or growth phases were measured in replicates (n=3-6, total of 26 conditions, Table S3). Quantified CL data for one sample per organism is depicted in analogy to Fig. 1B. The number of main CL species accounting for 95% of total CL mass is given as* $n_{CL95\%}$*.*

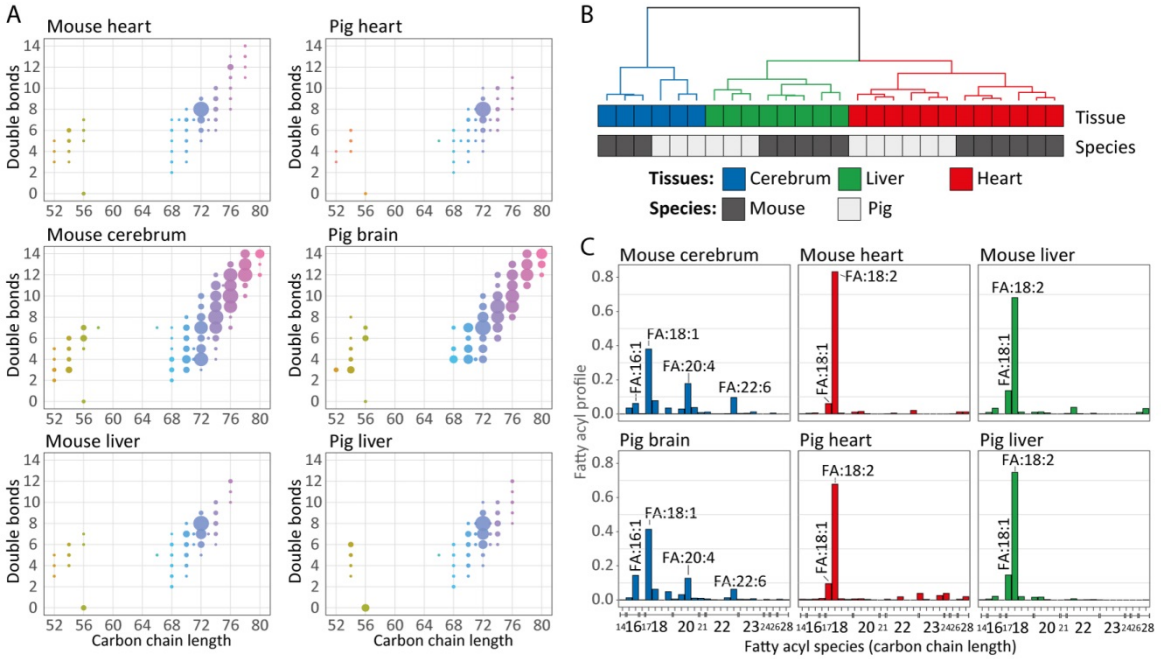

Supplemental Figure 16: ***Cardiolipin compositions in mouse and pig tissues****. (**A**) Representation of integrated raw data for cardiolipins extracted from heart, brain, and liver tissues of mice and pig tissues. Integrated peak areas of the first two cardiolipin isotope traces are added and projected back onto their respective carbon chain length and double bond components. Circle sizes indicate the cardiolipin species abundance in percent, fill color corresponds to the respective total number of side chain carbons. The internal standard (ISTD) is depicted as CL56:0. One representative plot per conditions is shown. (**B**) Hierarchical clustering analysis of cardiolipin profiles revealed strong co-clustering between tissues (Cerebrum: blue; liver: green; heart: red) and species specific differences were only secondary (Mouse: dark grey, pig: light grey). (**C**) Fatty acid profiles measured in mammalian tissues represented as means ± SD (n=3, biological replicates). High abundant fatty acids are additionally labelled (full profile can be found in Suppl Table 4).*

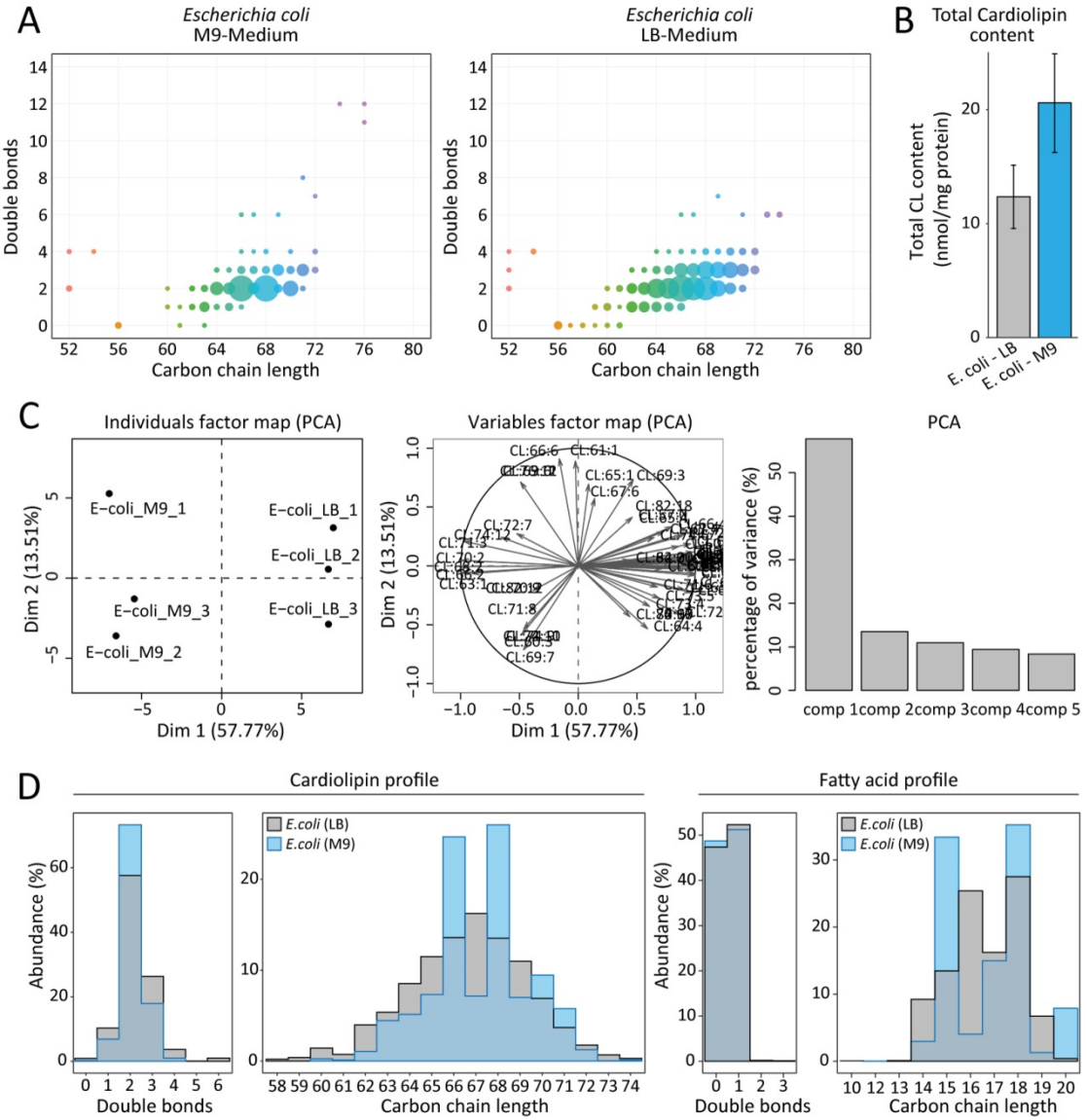

Supplemental Figure 17: ***Growth conditions dependence of E.coli cardiolipin composition****. (**A**) Representative illustration of one cardiolipin profile measured from E.coli lipid extracts after being grown in minimal M9 medium (left) and LB medium (right). Integrated peak areas of the first two cardiolipin isotope traces are added and projected back onto their respective carbon chain length and double bond components. Circle sizes indicate the cardiolipin species abundance in percent, fill color corresponds to the respective total number of side chain carbons. The internal standard (ISTD) is depicted as CL56:0. (**B**) Total cardiolipin content for the growth conditions as stated in (A) shown as mean ± SD (n=3). (**C**) Left: Principal components analysis (PCA) of E.coli cardiolipin compositions obtained in LB and M9 media. Cardiolipin profiles were used to construct a similarity matrix for PCA analysis. Component 1 and 2 captured 57.77% and 13.51% of the total variance, respectively, and sample groups were strongly separated along Component 1. Center:*

*Factor map of the PCA results indicates the contribution of individual cardiolipin species to the separation. Right: Fraction of total variance explained by Components 1-5. (**D**) Cardiolipin (left) and fatty acyl (right) profiles projected on their double bond count and carbon chain length components, respectively.*

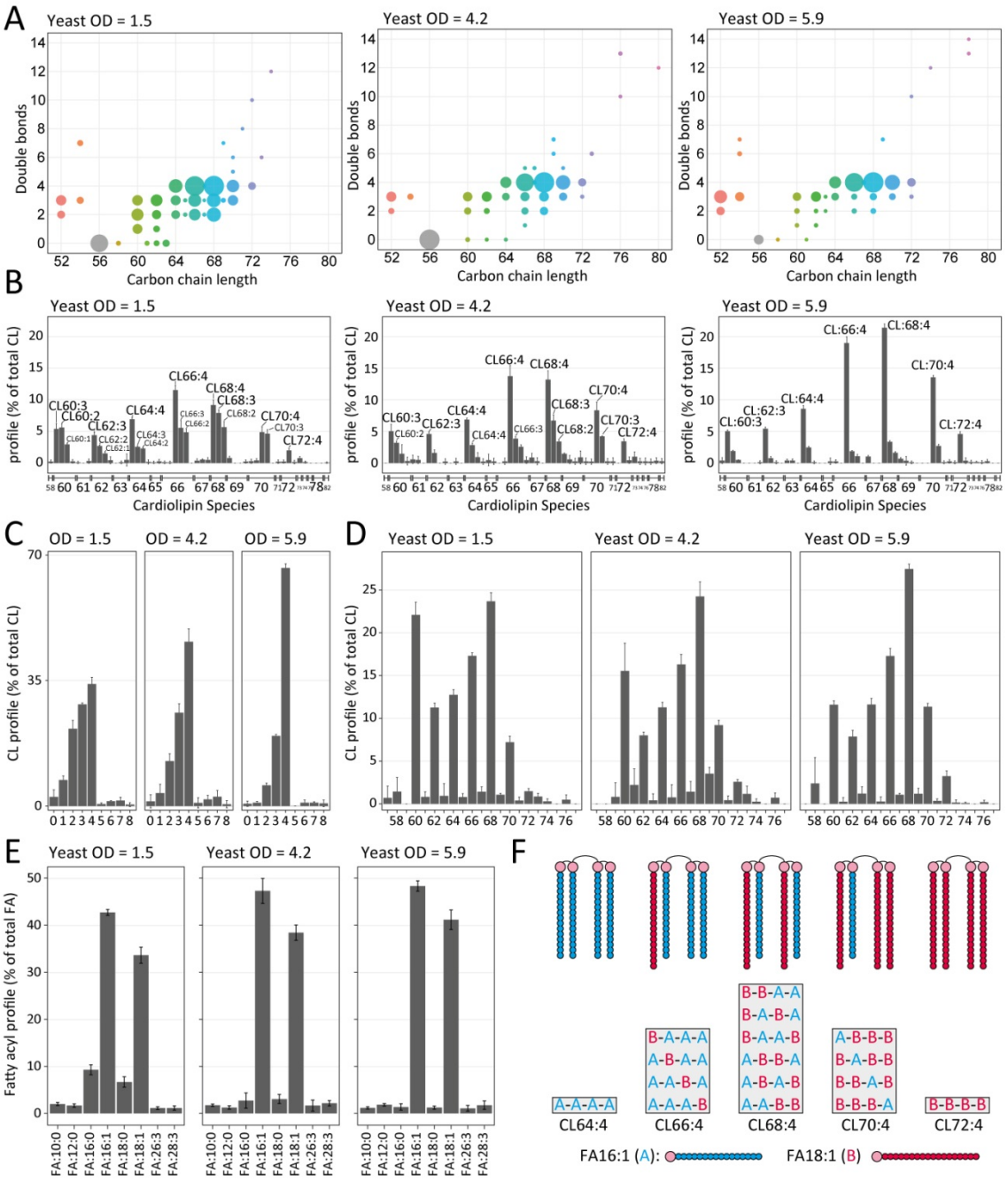

Supplemental Figure 18: ***Saccharomyces cerevisiae cardiolipin composition****. (**A**) MS1 data representation of the cardiolipin compositions recorded for yeast grown in batch culture and sampled at OD_{600} = 1.5, 4.2 (24 h) and 5.9 (48 h). One representative plot per condition is shown. Integrated peak areas of the first two cardiolipin isotope traces are added and projected back onto their respective carbon chain length and double bond components. Circle sizes indicate the cardiolipin species abundance in percent, fill color corresponds to the respective total number of side chain carbons. The internal standard (ISTD) is shown in grey. (**B**) Cardiolipin profiles for the same conditions stated in (A) shown as mean ± SD (n=4). (**C**) Cardiolipin data from (B) was*

*projected onto the respective double bond component. (**D**) Cardiolipin data from (B) was projected onto the respective carbon chain length component. (**E**) Fatty acyl profiles calculated from MS2 data for the same conditions stated in (A) shown as mean ± SD (n=4). Major fatty acids incorporated into yeast cardiolipins were FA16:0, FA16:1, and FA18:1. (**F**) Schematic representation of an entirely stochastic assembly of cardiolipin molecules from an equimolar pool of the two fatty acids FA16:1 (blue) and FA18:1 (red). The resultant profile is in good accordance with the yeast cardiolipin profile at OD_{600} = 5.9.*

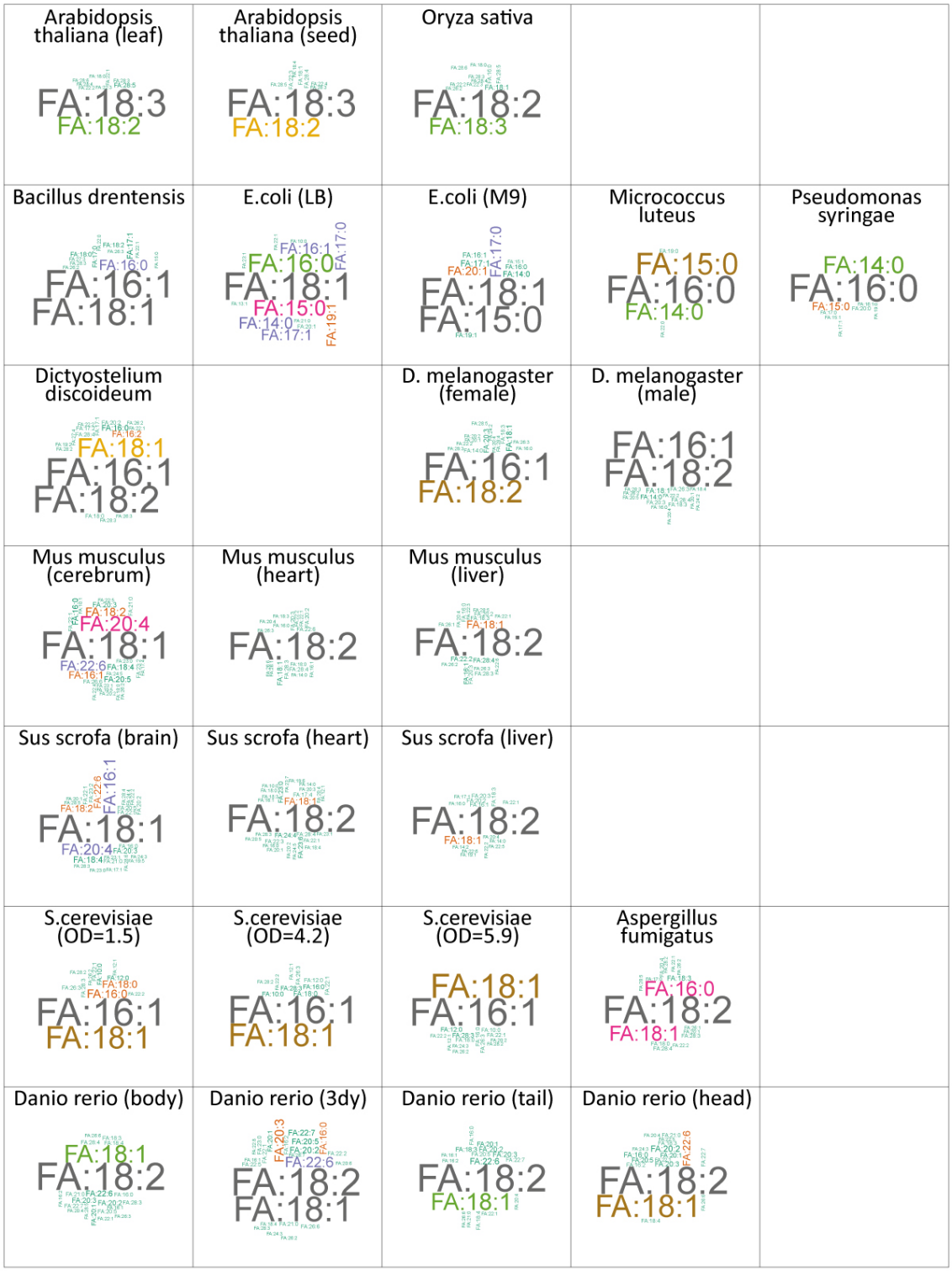

Supplemental Figure 19: ***Model organism fatty acyl compositions represented as wordclouds****. The fatty acid compositions incorporated into cardiolipins in 26 conditions/ tissues obtained from 13 different organisms are represented as wordclouds (see Suppl Table 4 for details). The size and color of the respective fatty acid indicates their relative abundance.*

Supplemental Table 1: Mammalian cell lines used in this study.

Cell line name	Growth condition				General cell line information						
	Medium	**Glucose (g/l)**	**Serum (%)**	**Passage**	**Biological source**	**Organism**	**Cell Type**	**Disease**	**Age**	**Gender**	**Comment**
Control 1	DMEM Gibco 21886	1	10%	p10	epidermal	Homo sapiens	Fibroblasts	control	33 years	female	
Control 2	DMEM Gibco 21886	1	10%	p3	epidermal	Homo sapiens	Fibroblasts	control	5 years	male	
Control 3	DMEM Gibco 21886	1	10%	p3	epidermal	Homo sapiens	Fibroblasts	control	1 year	male	
Control 4	DMEM Gibco 21886	1	10%	p16	epidermal	Homo sapiens	Fibroblasts	control	23 years	female	
Control 5	DMEM Gibco 21886	1	10%	p8	epidermal	Homo sapiens	Fibroblasts	control	32 years	female	NHDF (CC-2511, Lonza)
Control 6	DMEM Gibco 21886	1	10%	p6	epidermal	Homo sapiens	Fibroblasts	control	91 years	male	
Taz 1	DMEM Gibco 21886	1	10%	P9	epidermal	Homo sapiens	Fibroblasts	BTHS: c.718G>A (Gly240Arg)	unknown	male	
Taz 2	DMEM Gibco 21886	1	10%	p4	epidermal	Homo sapiens	Fibroblasts	BTHS: c.646G>A (p.G216R)	unknown	male	
Taz 3	DMEM Gibco 21886	1	10%	p4	epidermal	Homo sapiens	Fibroblasts	BTHS: c.684_685insC (p.227Phe_228Pro_fs)	unknown	male	

Supplemental Table 1 cont.: Mammalian cell lines used in this study.

Cell line name	Repl. scheme	Growth condition						General cell line information						
	() = sampled in parallel	Medium	Glucose (g/l)	Serum (%)	Passage	Additives	Estimated dublication rate (/h)	Biological source	Organism	Morphology	Disease	Age	Gender	Ethnicity
A431	(1)-(2)-(3)	VLE DMEM Biochrom FG1445	4.5	10	p7		0.95	skin/epidermis	Homo sapiens	epithelial	epidermoid carcinoma	85 years	female	
HEK	(1)-(2)-(3)	VLE DMEM Biochrom FG1445	4.5	10	p8		1.23	embryonic kidney	Homo sapiens	epithelial		fetus		
MCF7	(1-2-3)	EMEM30-2003 ATCC	1	10	p2	Insulin	0.33	mammary gland, breast; derived from metastatic site: pleural effusion	Homo sapiens	epithelial		69 years adult	female	Caucasian
A549	(1-2)-(3-4)	VLE DMEM Biochrom FG1445	4.5	10	p9		0.95	Lung	Homo sapiens	epithelial		58 years	Male	Caucasian
SK-N-SH	(1-2)-(3-4)	DMEM Gibco 31966	4.5	10	p19	Pyruvate	0.95	brain; derived from metastatic site: bone marrow	Homo sapiens	epithelial	neuroblastoma	4 years	female	
SKHep1	(1-2)-(3-4)	DMEM Gibco 31966	4.5	10	p4	Pyruvate	0.33	liver / ascites	Homo sapiens	endothelial		52 years	Male	Caucasian
T24	(1-2)-(3-4)	MEMAlpha Gibco 22561	1	10	p137		0.47	urinary bladder	Homo sapiens	epithelial	transitional cell carcinoma	81 years	female	Caucasian

K562	(1-2)-(3-4)	RPMI Sigma R8758	2	10	p2		0.57	bone marrow	Homo sapiens	lymphoblast	chronic myelogenous leukemia (CML)	53 years	female	
THP-1	(1-2)-(3-4)	RPMI Sigma R8758	2	10	p10	Mercaptoethanol 50 µM	0.33	peripheral blood	Homo sapiens	monocyte	acute monocytic leukemia	1 year infant	male	
Molt4	(1-2)-(3-4)	RPMI Sigma R8758	2	20	p4		0.33	T lymphoblast	Homo sapiens	lymphoblast	acute lymphoblastic leukemia	19 years	male	
U937	(1-2)-(3-4)	RPMI Sigma R8758	2	10	p6		0.33	pleural effusion	Homo sapiens	lymphocyte-like	histiocytic lymphoma	37 years	male	Caucasian
CHO-K1	(1-2)-(3-4)	F-12K Gibco 21127	1.26	10	p21		1.4	ovary	Cricetulus griseus	epithelial-like			female	
HL60	(1-2)-(3-4)	RPMI Sigma R8758	2.5	10	p4	10 mM Hepes, 1 mM Sodium pyruvat	0.33	peripheral blood	Homo sapiens	myeloblastic	acute promyelocytic leukemia	36 years	female	Caucasian
CaCo2	(1-2)-(3-4)	VLE DMEM Biochrom FG1445	4.5	10	p80		0.95	Colon	Homo sapiens	epithelial-like	Colorectal adenocarcinoma	72 years	Male	Caucasian
DLD1	(1-2)-(3-4)	RPMI Sigma R8758	2	10	p21		0.95	colon	Homo sapiens	epithelial	Dukes' type C, colorectal adenocarcinoma	adult	Male	
SH-SY5Y	(1-2)-(3-4)	DMEM Gibco 21886	1	10	p4	Pyruvate	0.47	bone marrow	Homo sapiens	epithelial	neuroblastoma	4 years	female	
Jurkat	(1)-(2)-(3)	RPMI Sigma R8758	2.5	10	p5	10 mM Hepes, 1 mM Sodium pyruvat	0.33	peripheral blood	Homo sapiens	lymphoblast	acute T cell leukemia		male	

Supplemental Table 2: Cell line Enrichment results - Results of hypergeometric probability analysis

	$P_{Total}=16$	$p_{Cluster\ A}=5$	$p_{Cluster\ B}=6$	$p_{Cluster\ C}=5$
		$s_{Cluster\ A}$	$s_{Cluster\ B}$	$s_{Cluster\ C}$
Q1	DMEM (s=7)	1	1	5
		0.97115	0.98951	0.0048077
Q2	RPMI (s=7)	3	4	0
		0.36538	0.18182	-
Q3	EMEM (s=1)	1	0	0
		0.31250	-	-
Q4	MEM (s=1)	0	1	0
		-	0.37500	-
Q5	high Glucose (s=6)	1	1	4
		0.94231	0.97378	0.03571
Q6	low Glucose (s=3)	1	1	1
		0.70536	0.78571	0.70536

Supplemental Table 3: Organism samples used in this study.

Organism	Organism part / Condition	Replicates	Background
Arabidopsis thaliana	Leaf	3	Locally supplied
	Seed	2	Locally supplied
Aspergillus fumigatus	with Iron	3	AfS77
	without Iron	3	AfS77
Bacillus drentensis	LB	3	DSM-15600
Danio rerio	Body	3	Wild-type AB Line
	Head	3	Wild-type AB Line
	Tail	3	Wild-type AB Line
	3 day post fertilisation	3	Wild-type AB Line
Dictyostelium discoideum	HL5	3	Ax4
Drosophila melanogaster	male	3	wildtype
	female	3	wildtype
Escherichia coli	LB	3	ATCC 11129
	M9	3	ATCC 11129
Micrococcus luteus	LB	3	
Mus musculus	Heart	6	C57BL/6J
	Liver	5	C57BL/6J
	Brain	3	C57BL/6J
Oryza sativa	Leaf	3	Locally supplied
Pseudomonas putida	LB	3	
Saccharomyces cerevisiae	OD=1.5	4	BY4741
	OD=4.2	4	BY4741
	OD=5.9	4	BY4741
Sus scrofa	Heart	3	Locally supplied
	Liver	3	Locally supplied
	Brain	3	Locally supplied

Supplemental Dataset S1: Organisms modeled fatty acyl composition ("Dataset S1 - Organisms fatty acyl composition.xlsx").

Supplemental Dataset S2:
Raw data have been deposited to the EMBL-EBI MetaboLights database with the identifier MTBLS636. All quantified data files have been deposited in the Mendeley Data repository (http://dx.doi.org/10.17632/kntnfm8grc.1) and are accessible in a browsable format at http://www.humgen.at/cardiolipin/" We used the following folder and file structure for each sample (*) and experiment:

[Plots]

****_profile.pdf***: Left panel: Relative quantified MS1 data projected back onto their respective carbon chain length and double bond components. Circle sizes indicate the cardiolipin species abundance in percent, fill color corresponds to the respective total number of side chain carbons. The internal standard (ISTD) $CL(14:0)_4$ is depicted as CL56:0. Right panel: Relative modelled fatty acyl abundance.

****_all_profiles.pdf***: Upper panel: Measurement and modeling analysis results for fatty acyl, phosphatidylglycerol, and cardiolipin profiles depicted as 2D-space (Carbon chain length against double bond number). Lower panel: Same profiles as above, but illustrated as bar graph.

****_fa_profile_QC.pdf***: Visual quality control for fatty acyl modeling results as described in Fig. 2H. PA profiles are computationally generated from FA composition results (blue bars) and are related to the PA profiles extracted from MS2 data (red bars) to evaluate the quality of fatty acyl modeling. The FA profile results explain PA patterns with high accuracy and were superior to an initial FA profile estimation that bases on projecting PA species on their main theoretical fatty acyls

****_ms1_output.pdf***: Quantified MS1 data depicted as described in Fig. 1B. Integrated peak areas of the first two cardiolipin isotope traces are added and projected back onto the m/z retention time graph. Circle sizes indicate the cardiolipin species peak areas, fill color corresponds to the respective total number of side chain carbons. The internal standard (ISTD) $CL(14:0)_4$ is shown in grey.

****_ms2_output.pdf***: Cardiolipin characterization in the respective sample including an absolute quantitative cardiolipin profile (left), and PA composition data projected onto the carbon chain length (center) and double bond count (right) components respectively (as described in Fig. 2F).

[Raw Data]

.mzML file: Raw data (Note to the editor: Not included in the initial submission due to large file sizes).

.csv file: MS1 analysis results obtained by identification and peak integration with MZmine2.

[Result Files]

_ms1_result.csv: MS1 analysis results including results for subsequent absolute quantification.

_ms12_result_short.csv: MS/MS structural cardiolipin modeling results projected onto the double bond and carbon chain length components respectively.

_ms12_result_long.csv: Complete MS/MS structural cardiolipin modeling results.

_fa_profile_data.RData: R-Object containing all analysed and modelled profiles for the different structural levels of a samples cardiolipin composition.

References

1. Liebisch G, et al. (2013) Shorthand notation for lipid structures derived from mass spectrometry. *J Lipid Res* 54(6):1523–1530.
2. Comte J, Maïsterrena B, Gautheron DC (1976) Lipid composition and protein profiles of outer and inner membranes from pig heart mitochondria. Comparison with microsomes. *Biochim Biophys Acta* 419(2):271–84.
3. Portero-Otín M, Bellmunt MJ, Ruiz MC, Barja G, Pamplona R (2001) Correlation of fatty acid unsaturation of the major liver mitochondrial phospholipid classes in mammals to their maximum life span potential. *Lipids* 36(5):491–8.
4. Lacombe C, Lubochinsky B (1988) Specific extraction of bacterial cardiolipin from sporulating Bacillus subtilis. *Biochim Biophys Acta* 961(2):183–7.
5. Schlame M (2008) Cardiolipin synthesis for the assembly of bacterial and mitochondrial membranes. *J Lipid Res* 49(8):1607–20.

EXTENDED PROTOCOL:

The molecular structural diversity of mitochondrial cardiolipins

Gregor Oemer[a], Katharina Lackner[a], Katharina Muigg[a], Gerhard Krumschnabel[b], Katrin Watschinger[c], Sabrina Sailer[c], Herbert Lindner[d], Erich Gnaiger[b], Saskia B. Wortmann[e], Ernst R. Werner[c], Johannes Zschocke[a], and Markus A. Keller[a,1]

[a]Division of Human Genetics, Medical University of Innsbruck, 6020 Innsbruck, Austria; [b]Oroboros Instruments Corporation, 6020 Innsbruck, Austria; [c]Division of Biological Chemistry, Biocenter, Medical University of Innsbruck, 6020 Innsbruck, Austria; [d]Division of Clinical Biochemistry, Biocenter, Medical University of Innsbruck, 6020 Innsbruck, Austria; and [e]Department of Paediatrics, Salzburger Landeskliniken, Paracelsus Medical University, 5020 Salzburg, Austria

[1]To whom correspondence should be addressed. Email: markus.keller@i-med.ac.at.

Biological material

Mammalian cell lines: see Supplemental Table 1: Mammalian cell lines used in this study ("Supplemental Table 1 - Mammalian cell lines.xlsx").

Model organism collection: see Supplemental Table 3: Organism samples used in this study ("Supplemental Table 3 - Organism samples.xlsx").

Reagents

Organic solvents are of HPLC grade or higher. Reagents should be of the highest grade available

- DMEM (Dulbecco's Modified Eagle Medium) low glucose (1g/l) (with GlutaMax™ and Sodium Pyruvate) (Gibco by Life Technologies, Carlsbad, USA, cat.no 21885-108)
- VLE-DMEM (Very Low Endotoxin-DMEM with stable glutamine, Biochrom GmbH, Berlin, Germany, cat.no FG 1445)
- EMEM (Eagle's Minimum Essential Medium, ATCC, Manassas, VA, USA, cat.no 30-2003)
- MEMalpha (Gibco by Life Technologies, cat.no 22561)
- RPMI (Sigma, Aldrich, cat.no R8758)
- F-12K (Ham's F-12K (Kaighn's) Medium, Gibco by Life Technologies, cat.no 21127)
- Panserin 401 without lipids (Serum-free All-round Medium with L-Glutamine, PAN BIOTECH, Aidenbach, Germany, cat.no P04-710401S2)

- Mitochondrial respiration medium: MiR05-Kit (OROBOROS INSTRUMENTS Corp, Innsbruck, Austria, Product ID: 60101-01, Lot# 0915)
- Trypan blue solution (0.4%, Sigma, Aldrich, cat.no T8154)
- LB-Agar (Roth, cat.no X965.2)
- Dialyzed fetal bovine serum (Invitrogen, Carlsbad, CA, USA, ct.no. 26400044)
- Fetal Calf Serum (FCS, Sigma Aldrich, St. Louis, USA – not heat activated, cat.no F7524)
- Antibiotics (Penicillin and Streptomycin, 17-602E, Lonza Group, Basel, Switzerland)
- Glutamine (100x, Invitrogen)
- Phosphate Buffered Saline (PBS, Serva Electrophoresis GmbH, Heidelberg, Deutschland, cat.no 47302.03)
- Isopropanol (IPA, 99.9%, Sigma Aldrich, St.Luis, MO, USA, cat.no 675431)
- Methanol (MeOH, 99.9%, Roth, Karlsruhe, Germany, cat.no 8388.6)
- Acetonitrile (ACN , HPLC grade, Fisher Scientific, Waltham, MA, USA, cat.no 1416033)
- Ammonium formate (≥ 99.0%, Sigma Aldrich, cat.no 70221)
- Formic acid (FA, 98%, Sigma Aldrich, cat.no 1.11670)
- Trypsin-EDTA (Sigma Aldrich, cat.no T4174)
- Chloroform (≥ 99.9%, Roth, cat.no 7331.2)
- O-Phosphoric acid (85%, Roth, cat.no 6366.1)
- Bovine Serum Albumin (BSA, Sigma Aldrich, cat.no A2058)
- 14:0 Cardiolipin (sodium salt), $CL(14:0)_4$ (Avanti Polar Lipids, Alabaster, AL, USA, cat.no 750332)
- 18:1 Cardiolipin (sodium salt), $CL(18:1)_4$ (Avanti Polar Lipids, cat.no 710335)

Equipment

- Mass spectrometer: Velos Pro Dual-Pressure Linear Ion Trap Mass Spectrometer (Thermo Fisher Scientific Inc, Waltham, USA)
- Chromatography: Dionex Ultimate 3000 HPLC (Thermo Fisher Scientific Inc, Waltham, USA)
- Quantitation software (MZmine2, http://mzmine.github.io/)
- Bench-top microcentrifuge (> 16.000 g, with cooling)
- Standard microplate UV/Vis-spectrophotometer (for protein concentration and lipid content assays)
- Agilent Poroshell 120 RO EC-C8 HPLC column (2.1 x 100 mm, 2.7um particle size, Agilent Technology, Santa Clara, CA, USA)
- Mixer mill for cell lysis (MM400, Retsch, Haan, Deutschland)
- Ultrasonic Bath

- Hand blender (Braun, Kronberg im Taunus, Germany)
- Rotavapor (Büchi Rotavapor R/A, Flawil, Switzerland)
- Neubauer counting chamber improved (Roth Karlsruhe, Germany, cat.no T729.1)
- Oroboros Oxygraph-2k (O2k, Oroboros Instruments, Austria; Gnaiger 2008)

Reagent setup

- **BSA stocks:** Dissolve 1 mg of BSA in 1 ml of 0.9% NaCl MQ-H_2O and store them in aliquots of 150 µl at -20°C. Add 1350 µl of 0.9% NaCl MQ-H_2O to the aliquot for each dilution series.
- **Internal Standard (ISTD) stock solution:** Dissolve $CL(14:0)_4$ (Tetramyristoyl-cardiolipin) in ethanol for 20 mM stock solution and store at -20°C. Prepare ISTD freshly for every extraction by diluting in a 2:1 chloroform:methanol solution to 0.5 µM, which is used for lipid extraction. Before diluting, bring to room temperature and check for complete resolution. Prepare 1 ml of extraction solvent for each sample.
- **Mobile phase A:** For 1 l mix 600 ml Acetonitrile and 400 ml H_2O (6:4 ratio) and add 630.6 mg ammonium formate (10 mM) and add 2 ml 99% formic acid (0.2% final concentration)
- **Mobile phase B:** For 1 l mix 900 ml isopropanol and 100 ml acetonitrile (9:1 ratio) and add 630.6 mg ammonium formate (10 mM) and add 2 ml 99% formic acid (0.2% final concentration)

Procedure

Sample Preparation

1. Preparing mammalian cell culture material.

A. Grow mammalian cells in 75 cm^2 cell culture flasks and incubate in a 5% CO_2 atmosphere at 37°C and 98% humidity.
B. When not otherwise stated use media containing 10% FCS (Fetal Calf Serum; F7524, Sigma Aldrich, St. Louis, USA – not heat activated) and 100 U/ml Pen-Strep (17-602E, Lonza Group, Basel, Switzerland).
C. Exact media compositions can be found in Supplemental Table 1.
D. Harvest cells at approximately 80-90% confluence.

2. Sampling of mammalian cell culture material.

A. Remove growth medium by aspiration and add 5 ml Trypsin-EDTA solution.
B. Incubate at 37°C for 5 min, then neutralized by adding of 5 ml medium or PBS.
C. Shake flask for cell detachment (control by light microscopy).
D. Transfer suspension into fresh Falcon vial and centrifuge at 800 rpm for 5 min.

E. Aspirate supernatant and resuspend the pellet in 1 ml 1x PBS solution and transfer into a 1.5 ml cryo-vial.
F. Centrifuge at 3300 x g for 5 min and aspirate supernatant.
G. Wash pellet by resuspending in additional 1 ml 1x PBS solution and repeat the centrifugation.
H. Remove supernatant and snap freeze the pellet in liquid nitrogen.
I. Store pellet at -80°C until lipid extraction.

3. Preparing bacteria material.

A. Streak *Escherichia coli* suspension from glycerol stock (ATCC 11129) on a LB-Agar plate.
B. Pick three single clone colonies and inoculate in 10 ml LB medium (X965.2, Roth Karlsruhe, Germany).
C. Grow pre-cultures by shaking at 200 rpm and 37°C overnight.
D. Generate main culture by transferring 0.15 OD_{600} units of these pre-cultures in an erlenmeyer flask and diluted to 100 ml LB or M9 (5 g NaCl, 30 g KH_2PO_4, 121.27 g Na_2HPO_4*$12H_2O$, 1 ml 1M $MgSO_4$, 100 µl 0.1M $CaCl_2$, 7.5 ml 20% glucose, 1 g NH_4Cl in 1 l H_2O), respectively.
E. Grow main cultures by shaking at 200 rpm and 37°C until $OD_{600} \geq 1.0$.
F. Collect pellets corresponding to 7.5 OD_{600} units by cold methanol precipitation (see Step 4).
G. For *Bacillus drentensis, Micrococcus luteus, Pseudomonas putida* use the same procedure, however grow then in LB medium only and at 30°C.

4. Cold methanol precipitation

A. This step orients along the procedure described in (1).
B. Withdraw 7.5 OD_{600} units of biomass and pipette the suspension into 20 ml MeOH in a 50 ml Falcon tube that has been tempered at < -40°C on dry ice.
C. Pellet the cells by immediate centrifugation at 3000 x g for 2 min in a pre-cooled centrifuge.
D. Decant the supernatant and remove the remaining methanol with a pipette.
E. Store the generated pellets at -80°C for subsequent lipid extraction (Step 14).

5. Preparing *Saccharomyces cerevisiae* material

A. Streak BY4741 yeast on a YPD-Agar plate (75 mg L-adenine-hemisulfate salt, 10 g Bacto yeast extract, 20 g Bacto Peptone, 20 g Dextrose, 20 g Bacto agar in 1 l H_2O).
B. Pick three single clone colonies and inoculate in 10 ml YNB medium (6.8 g Yeast Nitrogen Base, 40 g glucose in 1 l H_2O) and shake at 200 rpm at 30°C until solution becomes turbid.
C. Transfer aliquots of these pre-cultures to Erlenmeyer flasks containing 100 ml YNB Broth to obtain an OD_{600} of 0.15.

D. Shake at 200 rpm at 30°C and collect 7.5 OD_{600} units of biological sample material using the cold methanol precipitation method (Step 4) at the desired collection time points (12, 24 and 48 h).

6. Preparing mammalian tissue sample

A. *Mus musculus* samples were obtained from eight weeks old male and female C57BL/6J mice in biological triplicates, housed in microisolator cages under temperature controlled conditions and a 12 h light/dark cycle fed *ad libitum* (11% energy by fat, Ssniff Spezialdiäten GmbH, EF D12450B mod.)

B. Extract tissues using a scalpel and then immediately snap freeze them in liquid nitrogen.

C. *Sus scrofa* tissues were obtained freshly from a local butchery.

D. Homogenize mouse and pig tissue samples in PBS in a volume depending on the size of the tissue using an Ultraturrax mixer (Ika, Stauffen, Germany).

E. Avoid over-heating of the sample by placing it on ice and cross-over contamination by thoroughly washing the mixer after each use with 70% ethanol and water.

F. Determine the protein content of homogenates and use an sample amount 1 mg of protein for lipid extraction (Step 14). Homogenate can be stored at -80°C for several days.

7. Preparing *Danio rerio* sample

A. Keep zebrafish under standard conditions (2).

B. Collect adult fish and separate the head behind the gill and the tail behind the dorsal fin, then transfer the three generated parts (head, body, tail) into separate 1.5 ml cryo-vials.

C. Add 800 µl PBS and homogenize the tissues by using an Ultraturrax .

D. Freeze homogenates at -80°C until lipid extraction (Step 14).

E. Embryonic zebrafish were collected three days post fertilisation and samples were collected with the attached yolk.

F. These samples were directly frozen and stored at -80°C until lipid extraction (Step 14).

8. Preparing *Aspergillus fumigatus* sample

A. Start *Aspergillus fumigatus* cultures from spores and grow for 20 h at 37°C and 200 rpm in *Aspergillus* minimal medium (MM) according to (3) containing 1% glucose (carbon source), 20 mM glutamine (nitrogen source) with (+Fe/iron sufficiency) and without (-Fe/iron starvation) addition of 30 µM FeSO4. Wash the generated mycelia with PBS and collect by filtration.

B. Snap freeze and lyophilize the residue biomass and store at -80°C until lipid extraction (Step 14).

9. **Preparing plant sample material**

A. *Arabidopsis thaliana*, *Oryza sativa* plants were obtained from local providers.

B. Place seeds and green leaves separately into 2 ml flat bottom vials together with 400 µl MQ-H_2O and a 5 mm steel bead.

C. To achieve an initial homogenisation shake the vial at 30 Hz for 3 min.

D. Freeze homogenates at -80°C until lipid extraction (Step 14).

10. **Preparing *Drosophila melanogaster* material**

A. Grow flies at 60% humidity and 25°C in an artificial 12 h/12 h light/dark cycle according to (4).

B. Use sugar-cornmeal diet (110 g/l refined sugar, 52 g/l cornmeal, 27.5 g/l brewer's yeast, 4 g/l agar, 2.4 g/l tegosept dissolved in ethanol) as growth medium.

C. Collect male and female flies separately after 7 days.

D. 10-20 flies per samples were sufficient for performing all subsequent analysis steps.

E. Snap freeze samples and stored at 80°C until lipid extraction (Step 14).

11. **Preparing *Dictyostelium discoideum* material**

A. Cultivate the *Dictyostelium discoideum* Ax4 strain axenically in 9 cm cultures dish using HL5 medium, supplemented with 50 g/ml dihydrostreptomycin.

B. Grow adherent cultures from an initial density 5 x 10^4 cells/ml at 22°C and harvest at cell densities of 3-5 x 10^6 cells/ml.

C. Store pellets at -80°C until lipid extraction (Step 14).

12. Sample preparation for respirometry

A. Cell culture was performed as described in **1.** with following alterations:

B. Grow HeLa cells in 25 cm^2 flasks with either serum-free medium w/o lipids or serum-free medium w/o lipids supplemented with pig heart lipids for at least three days.

C. The sampling was performed until Step 2.D.

D. Aspire the supernatant, resuspend the pellet in 1 ml medium and count cells containing 1:2 trypan blue solution in a Neubauer counting chamber.

E. Resuspend 2-3 million cells in 300 µl mitochondrial respiration medium (MiR05) for permeabilized cells respiratory measurements and another 2-3 million cells in 300 µl cultivation medium (either Panserin 401 w/o lipids or with heart lipid supplementation) for intact cell respiratory measurements.

<u>Lipid extraction</u>

13. Protein quantification in homogenates:

A. Prepare a dilution series containing 1, 2.5, 5, 10, 15, 20, 25 and 30 µg/ml BSA in 0.9% NaCl.
B. Preload a 96-well microplate with 40 µl of Bradford reagent.
C. Add 160 µl of each standard and sample in technical duplicates.
D. Measure the absorption at 620 nm. If required dilute sample in 0.9% NaCl, so that absorbance values fall into the linear range.
E. Calculate sample concentrations by linear regression of the external dilution series readings.

14. Lipid extraction

A. For bacteria and mammalian cell pellets, add 200 µl MQ-H_2O and suspend pellet (Volume can be adjusted to fit the pellet size).
B. Add approx. 100 mg of glass beads and perform cell lysis by using a mixer mill four times at 20 Hz for 30 sec using a precooled block.
C. If required, withdraw 10 µl of suspension for protein quantification (Step 13).
D. Add 500 µl of 2:1 chloroform:methanol solution containing 0.5 µM of the ISTD.
E. Homogenize the mixture in the Mixer mill four times at 20 Hz for 30 sec using a precooled block.
F. Sonicate the mixture for 5 min in an ice cooled ultrasonic device and vortex additionally for 30 sec.
G. Centrifuge at 15,000 rpm at 4°C for 10 min to allow complete phase separation.
H. Transfer organic phase (bottom) into fresh glass vial.
I. Repeat extraction with the remaining water phase for a second time by adding additional 500 µl of extraction solvent containing the ISTD.
J. Dry the combined organic phases under a stream of N_2 gas or in a chemical hood overnight.
K. For other tissues the same extraction protocol is used with steps A-D being omitted.
L. The lipid extract can be stored at -20°C.

15. Lipid extraction of heart tissue for supplementation

A. Homogenize 20 g pig heart tissue (purchased at the local butchery) in 500 ml PBS using a hand blender.
B. Extract lipids thrice using 500 ml 2:1 chloroform/methanol mixture in a 1 l separating funnel.
C. Collect organic phases containing the lipid extract and evaporate in rotavapor at 40°C and 750 mbar.
D. Weigh dried lipid extracts, resuspend to 25 mg/ ml with 2:1 chloroform/methanol mixture and store in 2 ml aliquots in glass vials at -80°C.

16. Supplement media preparation

A. Bring 2 ml 25 mg/ml aliquot heart lipid extract (Step 15.D) to room temperature.

B. Remove 40 mg lipid extract and transfer to 250 ml glass bottle.
C. Evaporate solvent under N2 stream.
D. Add 200 ml lipid-free Panserin 401 and shake in water bath at 50°C for 24 h.
E. Filter supplemented medium through 0.2 µm pore filter for sterilization.
F. Store supplemented medium at 4 °C.

17. Sample dilution

A. Dissolve the lipid extracts in the mobile phase composition (38/62% running solvent A/B) and transfer to brown glass autosampler vials (usually in 50 or 100 µl).
B. For quality control, pool 5-10 µl of each sample to generate a QC sample.
C. Prepare Blank samples that consist of the starting composition of the mobile phase.

18. High-Resolution Respirometry - Mitochondrial function in intact and permeabilized cells (performed by Oroboros Instruments)

Oxygen consumption of HeLa cells was measured by High-Resolution Respirometry with the two chamber Oroboros Oxygraph-2k (O2k, Oroboros Instruments, Austria) and the software DatLab 7.1 for data acquisition and analysis. Four instruments were used in parallel. In each O2k, one chamber contained cells treated with Panserin 401 w/o lipids medium and the other chamber cells pre-treated with Panserin 401 medium with heart lipid supplementation. The 2-ml chambers were thermostatted at 37°C. Respiration medium was equilibrated with air for calibration of the oxygen sensors. After injection of 250 µl of cell suspension the closed chamber contained 1.5 – 2 x 10^6 cells and the oxygen range was maintained between air saturation and a minimum of 100 µM Oxygen flux [pmol $O_2 \cdot s^{-1} \cdot mL^{-1}$] was automatically corrected for instrumental background and results were expressed as oxygen flow per cell [amol $O_2 \cdot s^{-1} \cdot cell^{-1}$] (5)

In the experimental protocol for intact cells the respiratory medium was either Panserin 401 w/o lipids or with lipid supplementation. After stabilization of ROUTINE respiration the ATP synthase inhibitor oligomycin was added at a concentration of 2.5 µM and oxygen flow declinedto the level of LEAK respiration. The uncoupler carbonyl cyanide m-chloro phenyl hydrazine (CCCP) was titrated in steps of 0.5 – 1 µM until respiration reached the maximum level of electron transfer (ET) capacity. Finally, the Complex I inhibitor rotenone (1 µM) and Complex III inhibitor antimycin A (2.5 µM) were added, reducing respiration to residual oxygen consumption (ROX).

Two substrate-uncoupler-inhibitor titration (SUIT) protocols were applied to analyse mitochondrial respiratory capacity in various pathway control states of cells suspended in mitochondrial respiration medium (MiR05-Kit, Oroboros Instruments, Austria) (6). After measurement of ROUTINE

respiration in the intact cells, the plasma membranes were selectively permeabilized with 10 µg/ml digitonine, enabling full access of added substrates and toxins to the mitochondria. Following the decline of oxygen flow due to the loss of internal substrates to the extracellular environment, substrates and ADP were added successively for evaluation of oxidative phosphorylation (OXPHOS) capacity. In SUIT 1, fatty acid oxidation (F) was stimulated by 0.5 mM octanoylcarnitine and 0.1 mM malate. NADH-linked (N-linked) respiration was measured after further addition of 5 mM pyruvate and 10 mM glutamate. Maximum OXPHOS capacity was obtained with combined F-, N- and succinate-supported respiration (FNS-linked; 10 mM succinate), and 10 mM glycerophosphate (FNSGp-linked). This was followed by uncoupler titrations (FNSGp-linked ET-capacity), and inhibition of Complex I to obtain SGp-linked ET-capacity. Addition of antimycin A inhibited respiration to the level of residual oxygen consumption (ROX). Subsequently, the artificial Complex IV substrate N,N,N',N'-Tetramethyl-p-phenylenediamine dihydrochloride (TMPD, 0.5 mM; ascorbate, 2 mM) was injected, and after 20 min of chemical equilibration near air saturation CIV was inhibited by azide (100 mM). Auto-oxidation was subtracted from the total rate to obtain CIV activity (7).

In SUIT 2 permeabilization of cells was followed by adding pyruvate (5 mM) and malate (2 mM), supporting N-linked LEAK respiration in the absence of phosphorylation. ADP (2.5 mM) was added to induce N- OXPHOS-capacity. Cytochrome *c* (10 µM) was added to test for the intactness of the outer mitochondrial membrane. After injection of succinate (10 mM; NS-OXPHOS capacity), CCCP was titrated stepwise (NS-ET capacity), after which the addition of rotenone reduced respiration to S-ET capacity. Antimycin A was again added to obtain ROX.

LC-MS set-up

In this study, a Dionex Ultimate 3000 HPLC (Thermo Fisher Scientific Inc, Waltham, USA) combined with an Agilent Poroshell 120 RO EC-C8 column (Agilent Technologies, Santa Clara, USA) was used for the chromatographic separation of cardiolipins. The Velos Pro Dual-Pressure Linear Ion Trap Mass Spectrometer (Thermo Fisher Scientific Inc, Waltham, USA) was used for data-dependent acquisition of MS/MS spectra. In this mode, the acquisition software (Xcalibur™, Thermo Fisher Scientific Inc) continuously evaluates the full scan survey MS data as it collects and triggers the acquisition of MS/MS spectra depending on preselected criteria. In each cycle, one precursor ion with the highest intensity was selected for fragmentation.

19. Preparation of sample worklists

A. Set up the sequence of sample to start and end with Blanks and use them to rule out potential cross-contaminations. Also place a Blank after every 3-5 samples.
B. Measure one QC sample for every 6-10 samples in the sequence and a minimum of 5.

C. A 100 µl Blank sample should be used in a maximum of 5 times to avoid needle crossover contaminations.
D. Measure a dilution series of the two commercially available standards $CL(14:0)_4$ and $CL(18:1)_4$ with the six concentrations 12.5, 3.13, 0.781, 0.195, 0.0488, and 0.0122 µM (1:4 dilutions) at the beginning and the end of each batch used for retention time validation and cardiolipin quantification.

20. HPLC setup

A. Prepare running solvent A (60/40 Acetonitrile/H_2O, 10 mM ammonium formate, 0.2% formic acid) and running solvent B (90/10 Isopropanol/Acetonitrile, 10 mM ammonium formate, 0.2% formic acid) and degas for 10 min in an ultrasonic bath.
B. Purge all tubings with running solvent for 5 min for 5 min.
C. Set column oven to 50°C and equilibrate the column for at least 30 min at 0.4 ml/min in mobile phase starting condition (38/62% Buffer A/B).
D. Precool sample tray to 10°C before adding samples.
E. Injection volume was set to 10 µl.
F. For each sample run the HPLC gradient starts with 5 min isocratic 62% solvent B followed by a 7.5 min gradient to 74% solvent B. Next complete elution from the column is ensured with a step to 99% solvent B within 0.5 min for 4 min and subsequent re-equilibration at 62% solvent B min for 1.5 min. The flow rate was 0.4 ml/min for 13 min, then ramped up to 0.6 ml/min within 1.5 min and kept there for 2.5 min. For re-equilibration the flow rate was decreased back to 0.4 ml/ min within 0.5 min.

Table 1 HPLC parameters

MS system:	Thermo Scientific® LTQ Velos
LC system	Dionex® Ultimate 3000
Column	Agilent® Poroshell 120 RO EC-C8
Column oven temperature	50°C
Sampler temperature	10°C
Mobile Phase A	10 mM Ammonium formate 0.2% Formic acid in 60/40 Acetonitrile/Water
Mobile Phase B	10 mM Ammonium formate 0.2% Formic acid in

	90/10 Isopropanol/Acetonitrile
Flow rate	0.400 ml/min
Gradient	62% for 5 min
	62% to 74% in 7.5 min
	74% to 99% in 30 sec
	99% for 4 min
	99%-62% in 30 sec
	62% for 1.5 min
Sample loading	20 µl loop
Injection volume	10 µl
Wash volume	200 µl

21. MS set-up

A. Optimize all MS settings and ESI source parameters for high cardiolipin sensitivity (compare Table 2).
B. Before each sequence, calibrate the MS was in negative mode by autotuning on 1456.1 m/z using a diluted $CL(18:1)_4$ standard (Avanti Polar Lipids Inc., Alabaster, USA).
C. Perform data-dependent acquisition of CID fragment spectra by using a collision energy (CE) of 38 V. Optional: The parent mass selection process can be focused by a parent mass inclusion list (Table 3) pointing towards expected cardiolipin m/z and a permanent exclusion list with known instrument specific non-cardiolipin features.
D. After each MS2 scan the selected parent masses is added to a dynamic exclusion list for 8 seconds.
E. For each MS1 scan record (at least) one MS2 spectrum.

Table 2. Mass spectrometer settings - MS1 Method

Source	Electrospray ionisation
Capillary temperature	275°C

Source voltage	3.8 kV
Full MS mass range	1000-1600 (m/z)
Scan rate	Normal
Activation type	CID
Isolation width	1.50
Normalized Collision energy	38
Default charge state	1
Activation time	10 ms
MS2 mass range	5% – 105% relative to mass of parent
No. of microscans Full MS	3
No. of microscans MS2	5
Dynamic exclusion	enabled
Exclusion duration	8 s

Table 3. MS parent mass inclusion list (optional)

m/z	m/z	m/z	m/z	m/z	m/z
1239.9	1386.1	1420.0	1452.0	1485.0	1544.0
1261.9	1388.1	1422.0	1452.1	1488.0	1546.0
1316.1	1390.0	1424.0	1454.1	1490.0	1548.1
1318.0	1394.1	1426.1	1456.1	1492.0	1556.0
1320.0	1396.1	1428.1	1458.1	1494.0	1558.0
1329.9	1397.8	1430.1	1462.0	1498.0	1560.0
1332.0	1398.0	1432.1	1464.0	1500.0	1562.0
1344.0	1400.1	1436.0	1468.0	1502.0	1572.0
1346.0	1402.1	1438.0	1470.0	1504.0	1574.0
1348.1	1404.1	1440.1	1472.0	1507.0	1576.0

1350.1	1408.0	1442.1	1474.0	1514.0	1582.0
1358.0	1410.0	1444.0	1474.1	1516.0	1584.0
1360.1	1412.1	1444.1	1476.0	1518.0	1586.0
1362.1	1414.1	1446.0	1476.1	1520.0	1588.0
1370.0	1416.1	1446.1	1478.0	1527.0	1594.0
1372.1	1416.1	1448.0	1478.1	1530.0	
1374.0	1418.0	1448.1	1480.1	1532.0	
1376.1	1418.1	1450.0	1482.1	1534.0	
1384.1	1420.0	1450.1	1484.1	1542.0	

Data analysis

22. Conversion of raw data

A. For subsequent analysis, convert all generated RAW files into the open source *.mzML format by using the MSConvertGUI application (http://proteowizard.sourceforge.net/). This step ensures compatibility of subsequent analysis steps with mass spectrometric data from diverse manufacturers.

23. Peak integration and data analysis

A. Perform the initial analysis of mzML files with the open-source software MZmine2 (Version 2.2.21, http://mzmine.github.io/).

B. Crop the relevant regions of each dataset (Raw data methods/ Filtering/ Crop filter: 1.8-12.5 min, 1000-1600 m/z) and baseline-correct the data (Raw data methods/ Filtering/Baseline correction: TIC, 0.2 m/z bin with, asymmetric baseline corrector: 100,000,000 smoothing, 0.5 asymmetry factor). A batch analysis pipeline with these parameters can be created for automatization.

C. Identify and integrate all cardiolipin peaks in each sample by targeted peak detection using a curated cardiolipin peak list (Raw data methods/ Peak detection/Targeted peak detection).

D. This peak list contains m/z and retention time information for up to 135 cardiolipins and 35 monolyso-cardiolipins and their first isotope peaks that have been identified throughout all measured samples.

E. In order to compensate for retention time- and m/z-shifts, subject a template peak list to calibration using the retention time and m/z information measured for the ISTD ($CL(14:0)_4$) and the $CL(18:4)_4$ peak in the respective sample. Perform this step by linear regression analysis and using the R environment (http://www.r-project.org/).

F. Set the following parameters for targeted peak detection: 100% intensity tolerance, 0.15 m/z or 50 ppm m/z tolerance and 0.2 min retention time tolerance. Adjust the noise level depending on the individual sample noise level in the range of 400 to 800. Check correct integration by visual inspection and manually correct or adjust integration parameters if necessary. Export sample specific peak lists as CSV files for documentation purposes.

G. Export the resultant integrated peak area data for all features from MZmine2 as CSV result files.

24. Quantification of cardiolipins from MS1 data

A. Unless otherwise stated, conduct all subsequent data analysis steps in the open source R environment (http://www.r-project.org/) (8).

B. Sum up the peak area data obtained for the monoisotopic mass with their respective first isotope peak areas.

C. Use the dilution series of cardiolipin standards (Step 19D) to convert peak areas into concentration values using a linear regression model with logarithmic transformations.

D. When applicable, use the internal standard measurement values for each individual sample to adjust for potential dilution errors.

E. Normalize the obtained concentration data to the respective protein content in samples, which has been measured in parallel (see Step 13).

25. Mathematical modeling of cardiolipin structural information from MS2 data

A. Perform analysis steps as described in the Supplemental R-Script 1.

B. This analysis bases on the MS2 spectra containing mzML file (Step 22), the quantified cardiolipin MS1 results (CSV file derived from Step 23), mass tolerance information describing the mass accuracy and resolution of the mass spectrometer used, as well as the boundaries for carbon chain length and double bond count of expected PG fragments.

C. Import mzML data by using the *mzR* R-package (9).

D. Annotate the recorded MS2 fragment spectra according to their corresponding MS1 cardiolipin peak window to identify the parent cardiolipin species and filter for relevant MS2 spectra.

E. Construct a list of all theoretically possible PG monomers within the double bond range [0, 15] and the carbon side chain length range [20, 50]. Calculate three m/z values for each PG following the major fragmentation paths.

F. Use the constructed theoretical fragment list to construct a fragment annotation matrix by grouping fragments to unique masses according to the instruments mass tolerance.

G. Form the scalar product of the fragment annotation matrix with a vector describing the relative efficiencies of the individual fragmentation paths $[a_{f1}\ a_{f2}\ a_{f3}]$. This allows

predicting a fragmentation pattern y_{theo} from a given PG profile $PG_{theo} = [x_1\ x_2\ x_3\ \dots\ x_z]$ and thus serves as the crucial set of constraints required for an automated analysis of MS2 spectra (see equation (1)).

$$y_{theo} = \begin{bmatrix} y_{theo_1} \\ y_{theo_2} \\ \dots \\ y_{theo_{(z+n-1)}} \end{bmatrix} = \begin{bmatrix} x_1 & 0 & 0 \\ \dots & \dots & \dots \\ x_m & x_1 & 0 \\ \dots & \dots & \dots \\ x_n & x_m & x_1 \\ \dots & \dots & \dots \\ x_z & x_n & x_m \\ \dots & \dots & \dots \\ 0 & x_z & x_n \\ \dots & \dots & \dots \\ 0 & 0 & x_z \end{bmatrix} \cdot \begin{bmatrix} a_{f1} \\ a_{f2} \\ a_{f3} \end{bmatrix} \quad (1)$$

H. Convert the individual MS2 spectra into a vector y_{obs}, following same logical format as y_{theo} by annotating of normalized peak intensities in a mass tolerance dependent manner. If required conduct a previous mass calibration of MS2 spectra using the fragments recorded for the internal standard $CL(14:0)_4$.

I. Construct the final minimization function as the euclidean distance between the theoretical fragmentation model y_{theo} and the reformatted MS2 spectrum y_{obs}(Equation 2).

$$d(y_{theo}, y_{obs}) = \sqrt{\sum_{i=1}^{n} (y_{theo_i} - y_{obs_i})^2} \quad (2)$$

J. Apply the general-purpose optimization function *optim* to minimize equation (2) over the parameters $[x_1\ x_2\ x_3\ \dots\ x_z]$ and $[a_{f1}\ a_{f2}\ a_{f3}]$. As initial values for $[x_1\ x_2\ x_3\ \dots\ x_z]$ use y_{obs}in the range [1, z] and the ratio 10:1:3 for the fragmentation path efficiencies.

K. Run the *optim* function using the L-BFGS-B method which is utilizing the limited-memory modification of the BFGS quasi-Newton algorithm (10). Set the box constraints to [0, 1] in order to account for the profile-nature of the parameters to be optimized.

L. For each MS2 spectra a modeled PG profile is obtained as a result. This includes an annotation with the respective parent cardiolipin species, and the total MS2 intensity values.

M. In order to obtain a PG profile for each cardiolipin species, all solved profiles are weighted according to their MS2 intensities and summed up. If required for illustration purposes project the resultant condensed PG profiles onto their respective double bond and side chain carbon components.

26. FA profile modeling

A. Fatty acyl side chain distributions are modeled following an analogue approach as described above (Step 25).
B. Construct a vector describing the available fatty acyl space $FA_{theo} = [FA_1\ FA_2\ FA_3\ \ldots\ FA_n]$ on basis of boundaries for carbon chain length [10, 28] and the number of double bonds [0, 8].
C. From this fatty acid list calculate all unique dual combinations to obtain a PG profile $PG = [PG_1, PG_2, \ldots,\ PG_n]$describing the theoretically available PG space.
D. Generate a function to calculate PG_{theo}, where each vector element is constructed from all relevant relative fatty acid abundances according to: $PG_k = \Sigma\ FA_i \cdot FA_j$ for all combinations fulfilling the condition $i + j = k$ in terms of carbon chain length and double bond number.
E. To generate PG_{obs} annotate the structure of PG_{theo} with the result profile $[x_1\ x_2\ x_3\ \ldots\ x_z]$ from Step 25.
F. In analogy Step 25, minimize the euclidean distance (Equation 2) between $PG_{obs}$and PG_{theo} over the parameters $FA_{theo}$by using the optim function with [0, 1] box constraints and the L-BFGS-B Method. Estimate the initial values for $FA_{theo}$from $PG_{obs}$by distributing PG abundances to fatty acyls according to equation (3), which generates the closest pair of fatty acids with even carbon numbers and maximum double bond symmetry.

$$PG\ X : Y \rightarrow FA\left(2 \cdot \left\lfloor \frac{X}{4} \right\rfloor\right) : \left\lfloor \frac{Y}{2} \right\rfloor + FA\left(2 \cdot \left\lceil \frac{X}{4} \right\rceil\right) : \left\lceil \frac{Y}{2} \right\rceil \qquad (3)$$

G. Fatty acyl profiles can be either solved from cumulative PG profiles describing the PG composition in a sample, or for PG compositions of a single cardiolipin species.

References

1. Koning W de, Dam K van (1992) A method for the determination of changes of glycolytic metabolites in yeast on a subsecond time scale using extraction at neutral pH. *Anal Biochem* 204:118–123.
2. Westerfield M (2007) *The Zebrafish Book. A Guide for the Laboratory Use of Zebrafish (Danio rerio)*. 5th Ed.
3. PONTECORVO G, ROPER JA, HEMMONS LM, MACDONALD KD, BUFTON AWJ (1953) The genetics of Aspergillus nidulans. *Adv Genet* 5:141–238.
4. Sebald J, et al. (2016) Impact of the Chromatin Remodeling Factor CHD1 on Gut Microbiome Composition of Drosophila melanogaster. *PLoS One* 11(4):e0153476.
5. Gnaiger E (2008) Polarographic Oxygen Sensors, the Oxygraph, and High-Resolution Respirometry to Assess Mitochondrial Function. *Drug-Induced Mitochondrial Dysfunction* (John Wiley & Sons, Inc., Hoboken, NJ, USA), pp 325–352.
6. Gnaiger E, Kuznetsov AV, Schneeberger S, Seiler R, Brandacher G, Steurer W MR (2000) Mitochondria in the cold. In: Life in the Cold (Heldmaier G, Klingenspor M, eds). *Springer*:Heidelberg, Berlin, New York:431-42.
7. Doerrier C, et al. (2018) High-Resolution FluoRespirometry and OXPHOS protocols for human cells, permeabilized fibres from small biopsies of muscle and isolated mitochondria. *Methods Mol Biol* (in press).
8. R Core Team (2013) R: A Language and Environment for Statistical Computing. Available at: http://www.r-project.org/.
9. Chambers MC, et al. (2012) A cross-platform toolkit for mass spectrometry and proteomics. *Nat Biotechnol* 30(10):918–920.
10. Byrd RH, Lu P, Nocedal J, Zhu C (1995) A Limited Memory Algorithm for Bound Constrained Optimization. *SIAM J Sci Comput* 16(5):1190–1208.